Convergent cellular adaptation to a quiescence-like state in response to freeze-thaw stress

Charuhansini Tvishamayi[1,✉], Farhan Ali[3,*], Nandita Chaturvedi[1,*], Nithila Madhu-Kumar[1], Zeenat Rashida[4], Ankita Ray[1], and Shashi Thutupalli [1,2,✉]

[1]Simons Centre for the Study of Living Machines, National Centre for Biological Sciences (TIFR), Bangalore, India; [2]International Centre for Theoretical Sciences (TIFR), Bangalore, India; [3]Biodesign Center for Mechanisms of Evolution, Arizona State University, Tempe, AZ-85281, USA; [4]Institute for Stem Cell Science and Regenerative Medicine, Bangalore, India; [*]Equal Contribution, listed alphabetically

Rapid freeze-thaw is an extreme mechano-chemical perturbation that results in very low survival of many organisms (as low as a fraction of a percent). Here, using experimental evolution, we show that the budding yeast, *Saccharomyces cerevisiae* can adapt to freeze-thaw stress in a stereotyped manner, with survival increasing nearly two orders of magnitude from ≈2% to ≈70% in about 25 cycles of stress exposure. Adapted cells exhibit reduced membrane damage, smaller sizes, higher mass densities, and a lower prevalence of budding. Rheological measurements show that the adapted cells are stiffer and exhibit lower particle mobilities within the cytoplasm. Whole genome sequencing indicates that increased survival is not accompanied by specific (unique) genetic changes, but rather is associated with multiple, distinct genotypes. Concomitant with mechanical changes in the adapted cells, the basal intracellular level of trehalose, a sugar speculated to play a physical role in maintaining membrane and cytoplasmic integrity, exhibits a three-fold increase. Together, these cellular attributes strongly correlate with the entry of cells into a quiescence-like state. A quantitative model that incorporates selection based on cellular quiescence recapitulates the adaptation dynamics, *i.e.* increase in survival and trehalose levels, seen in experiments. Finally, we find that the evolved mechano-chemical phenotypes are similar even when we use qualitatively different freeze-thaw selection protocols for the evolution, hinting at a convergent adaptation.

Correspondence: ***charuhansini@ncbs.res.in; shashi@ncbs.res.in***

Introduction

Extreme environmental fluctuations perturb the mechano-chemical properties of cells and affect their fitness. Freeze-thaw is one such extreme perturbation that significantly affects the survival of cells. During freezing, cells experience many sharp transitions — mechanical changes, changes to the metabolic state, nutrient uptake, respiration etc. — that likely result in low survival of many cells. Among other factors, survival strongly depends on the speed of freezing and thawing. Several studies have found that rapid freezing (followed by thawing) in particular leads to significantly low survival in several species (1; 2; 3; 4), and can be as low as a fraction of a percent for *Saccharomyces cerevisiae* at high freezing rates ($>$ 10 K/min) (1).

A few previous studies on freeze-thaw tolerance have focused on identifying chemical changes in the cell in response to freeze-thaw stress. These studies identified molecular/genetic factors such as tpi1, erg10, hsp12, alpha-ketoglutarate, trehalose responsible for freeze-thaw tolerance (5; 6; 7; 8). Other studies have associated certain classes of molecules such as sugars (trehalose, glucose, sucrose) and intrinsically disordered proteins (IDPs) or macromolecules with increased tolerance to freeze-thaw (9; 3; 10; 11; 12), hypothesizing that these kinds of molecules could increase cytoplasmic macromolecular crowding (and reduced intracellular water) and thereby facilitate survival.

Previous studies have also implicated trehalose, a dimer of glucose, to aid in survival to different types of environmental stresses such as desiccation or freeze-thaw (13; 14; 15; 16). Chen *et al.* have shown that externally increasing trehalose concentration in *Saccharomyces cerevisiae* is sufficient to confer increased tolerance to freeze-thaw (9). Trehalose has been hypothesized to protect membranes (17), proteins (18) and support reduced fluidity of the cytoplasm.

Cytoplasmic stiffening *i.e.* reduced fluidity is a rheological state that is observed in cellular response to diverse environmental stresses (19; 20; 21). Parry *et al.* (19) suggest that lack of cellular or metabolic activity leads to a decrease in fluidity of the cytoplasm. Delarue *et al.* (21), have shown that increasing ribosome concentration decreases cytoplasmic fluidity and that the cell can actively tune ribosome concentration in response to the external environment. This suggests that the cell can tune cytoplasmic rheology via macromolecular crowding, which could in turn affect chemical reaction rates and hence cellular or metabolic activity. External environmental stresses have also been shown to decrease cytoplasmic fluidity (22; 23; 24). These examples suggest that the cytoplasmic rheology can be actively tuned in response to environmental perturbations and that decreased cytoplasmic fluidity could help the cell retain its structure and organisation to aid survival/function. However, these changes may not reflect adaptations in an evolutionary sense.

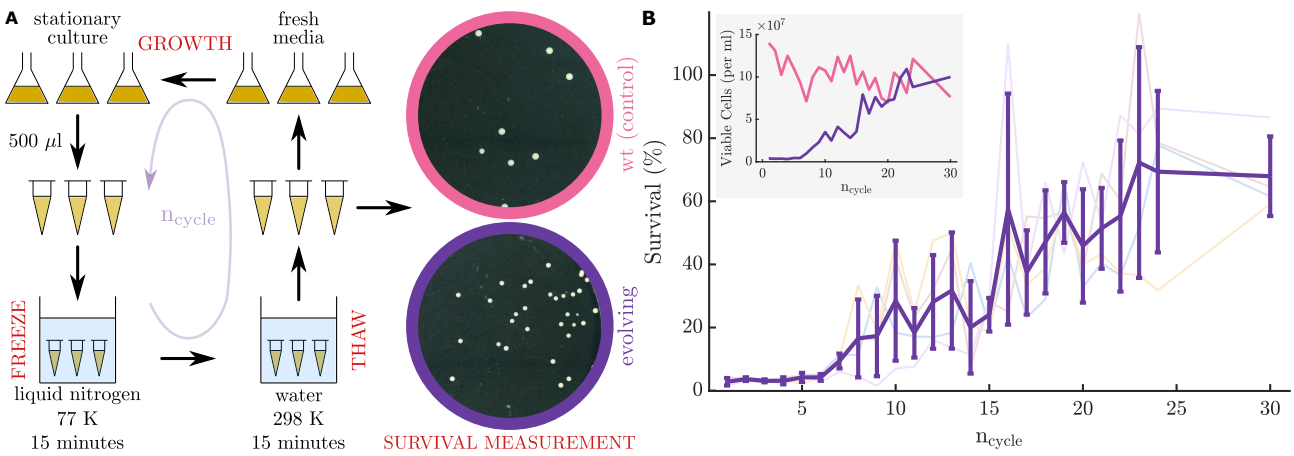

Figure 1. Experimental evolution can be used to increase survival of yeast under freeze and thaw stress. A Experimental design of selection for freeze-thaw tolerance. **B** Survival fraction of cells after freeze-thaw over the course of evolution. Inset: Number of viable cells after every freeze-thaw-growth cycle. Purple - evolving population. Pink - control population.

Previously, lab evolution studies which obtained freeze-thaw tolerant populations of *E. coli* and *L. rhamnosus* found that a cls mutant maintained membrane fluidity after a freeze-thaw (25; 26) without identifying other cytoplasmic characteristics, as described above, of the adaptations.

In this work, we ask if cellular mechano-chemical adaptations can be encoded *de novo* when cells undergo selection following repeated exposure to stress. In order to perform such a selection, cells need to be exposed to a stress that directly affects their survival, using which an experiment can be performed to ask if mechanical adaptations accrue over generations to aid survival. When *Saccharomyces cerevisiae* populations are exposed to fast freezing (> 10 K/min to -196 C) followed by thawing to room temperature, only about 2% of cells survived and therefore, we used this as a strong selection for cell survival. Yeast is also a useful model to perform an experimental evolution since it (a) has a low doubling time and survival can be measured reliably, (b) is a large enough cell to image even the intracellular dynamics quantitatively, (c) is a well studied organism biochemically and genetically, and (d) its survival to freeze-thaw and trehalose correlations with freeze-thaw tolerance have been well characterised (1; 9; 27; 28).

We selected for freeze-thaw tolerance in *Saccharomyces cerevisiae* using multiple independent lines and characterized the differences between the wild type (WT, control) *Saccharomyces cerevisiae* strain and the freeze-thaw adapted (evolved) strain. We found that the freeze-thaw tolerant cells are smaller, lighter and denser and incur reduced membrane damage after a freeze-thaw. In addition, we observed increased basal intracellular trehalose concentrations, higher cellular stiffness and decreased cytoplasmic mobility in all freeze-thaw adapted populations. These various cellular attributes correlate with the characteristics of quiescence, a long-lived stress-tolerant state (29), suggesting that entry into a quiescence-like state could facilitate the cellular adaptation. We therefore developed a quantitative model for a trehalose based selection for quiescent cells, and indeed found that it recapitulates the experimentally seen adaptation dynamics. Finally, while each independent line resulted in different genetic mutations, these different genotypes however presented the same mechano-chemical phenotype, even when we use qualitatively different freeze-thaw selection protocols for the evolution, strongly hinting at convergent adaptation.

Results

A. *Saccharomyces cerevisiae* adapts to freeze-thaw stress

We first establish an experimental protocol in order to perform the selection (Fig. 1**A**). It is known that the survival of *Saccharomyces cerevisiae* upon freeze-thaw depends on the rate of freezing and thawing. Survival has been found to be minimal when it undergoes a fast freeze (> 10 K/min) to -196°C (1). We chose this regime to work in to possibly achieve the most significant increase in survival after adaptation. Before proceeding, we determined the effect of duration at -196°C on survival by exposing the WT (CEN.PK a/ α) stationary phase cell cultures to a fast freeze (> 10K/min) to -196°C and allowed them to remain at -196°C for varying lengths of time before thawing. Freezing was done by immersing 500 μl of stationary phase culture in 1.5 mL tubes in liquid nitrogen (-196°C) and the cultures were then thawed by immersing them in 25°C water for 15 minutes. We note that the survival fraction of yeast does not vary with duration at -196°C, as shown in Fig. S1. Therefore, for experimental convenience, we used a freeze duration of 15 minutes and selected for freeze-thaw tolerance at high cooling rates (> 10 K/min). The cells that survived the freeze-thaw were grown in fresh media until stationary phase (24 hours, ≈4 generations) and this cycle repeats. The survival fraction was then measured by colony forming units (CFUs). This cycle of freeze-thaw followed by growth was repeated until the survival fraction stopped increasing. For controls, the same protocol was followed without the freeze-

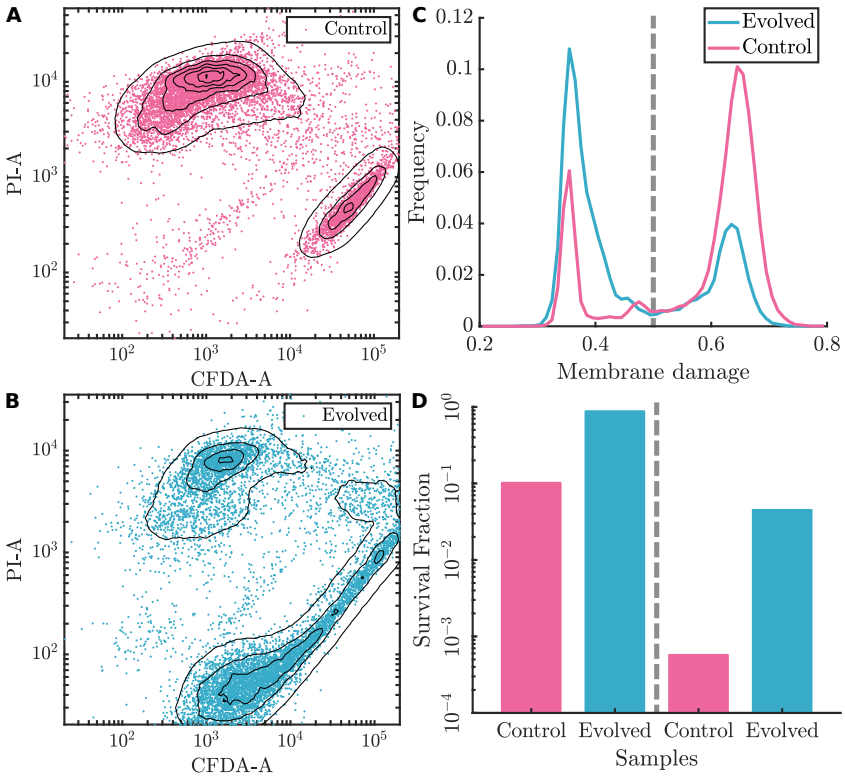

Figure 2. Freeze-thaw tolerant cells undergo reduced membrane damage and survive membrane damage A Flow cytometry measurements on Wild Type cells. Each point represents a single cell and the plot contains data for 10000 cells. The x-axis is the fluorescence intensity in the 5-CFDA channel. The y-axis is the fluorescence intensity in the propidium iodide channel. The contour lines represent changes in probability density of cells. The cluster on top comprises membrane damaged cells and the cluster at the bottom comprises cells with intact membranes. **B** Flow cytometry measurements on freeze-thaw tolerant cells. Each point represents a single cell and the plot contains data for 10000 cells. The x-axis is the fluorescence intensity in the 5-CFDA channel. The y-axis is the fluorescence intensity in the propidium iodide channel. The contour lines represent changes in probability density of cells. The cluster on top comprises membrane damaged cells and the cluster at the bottom comprises cells with intact membranes. **C** Distribution of membrane damage in cells calculated from plots A and B. **D** Viability of cells measured after sorting the two clusters found in plots A and B.

thaw procedure. To start the experiments, a single yeast colony was picked from an agar plate and grown as liquid culture to stationary phase. This starter culture was divided into six parts — two for controls and four biological replicates for selection.

Under this selection regime, the survival fraction increased from ≈2% up to an average of ≈70%, with one of the replicates as high as 85%, in only a span of ≈25 freeze-thaw cycles (Fig. 1**B**). This shows that the yeast cells can indeed adapt to freeze-thaw and next we proceeded to characterize the differences in the evolved strain with respect to the WT.

B. Freeze-thaw tolerant cells undergo reduced membrane damage

Membrane damage has been implicated as the primary cause of death after freeze-thaw (30; 31; 32). We therefore started by investigating if the freeze-thaw tolerant cells have a membrane-damage related adaptation. The presence or absence of membrane damage was measured by staining with two dyes — 5-carboxyfluorescein diacetate (5-CFDA) and Propidium Iodide (PI) — and measuring the intensities of fluorescence of both dyes using flow cytometry (Fig. 2**A,B**). Each point on these plots represents a single cell. The fluorescent form of CFDA leaks out of a cell quickly if it is membrane damaged. PI permeates cells with damaged membranes. Taken together, these dyes allow a clear distinction between membrane damaged cells and cells with intact membranes showing up as two distinct clusters in the data (Fig. 2**A,B**). We compute a single metric that combines this information to estimate the total membrane damage (using eq. S1), which clearly indicates that a smaller fraction of freeze-thaw tolerant cells undergoes membrane damage after freeze-thaw (Fig. 2**C**).

Further, to understand whether viability is dependent on membrane damage, we used fluorescence-activated cell sorting (FACS) to sort the population of cells into membrane-damaged and membrane-intact fractions to measure their viability (Fig. 2**D**). We find that the survival fraction of freeze-thaw tolerant cells within the membrane-damaged sub-population exceeds the wild type by about two orders of magnitude. Similarly, the viability of freeze-thaw tolerant cells with intact membranes is an order of magnitude higher than the corresponding wild type population. Membrane integrity can be associated with altered composition which can not only affect cell density but also morphology (33). Therefore we next probed the morphology and density of freeze-thaw tolerant cells at the point in their population growth stage, *i.e.* stationary phase, that we impose the freeze-thaw stress.

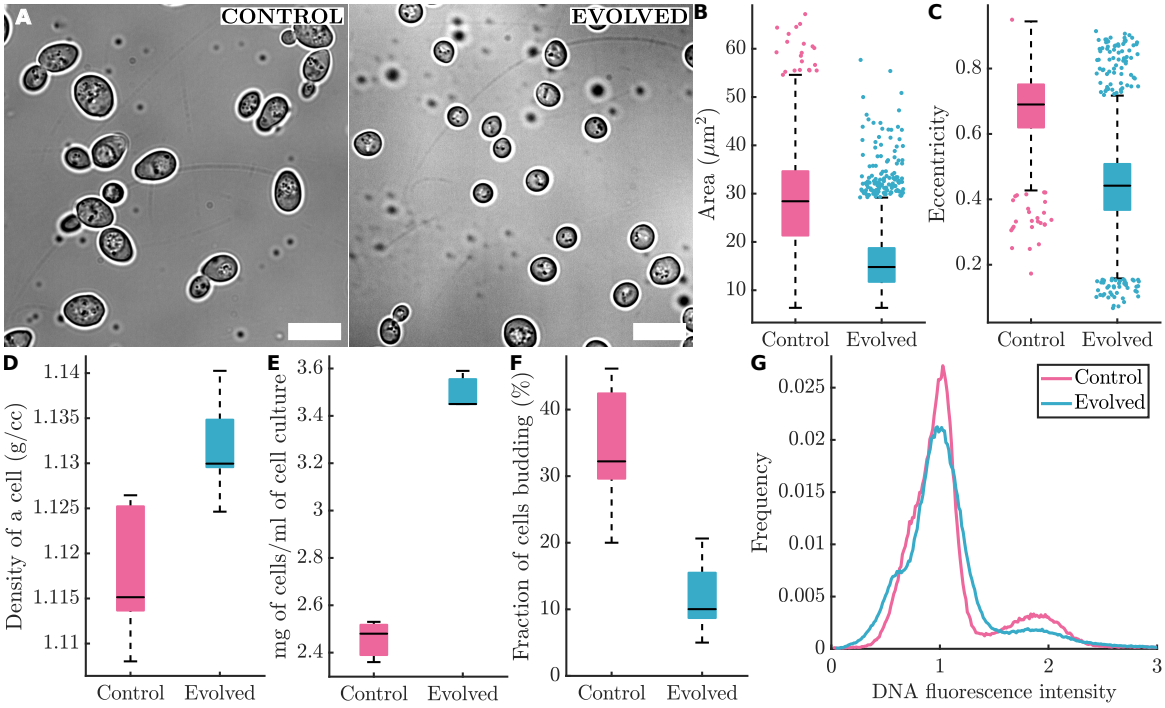

Figure 3. Cells of the population adapted to survive freeze and thaw are smaller, denser and exhibit reduced budding A Brightfield image of cells. Scale bar - 10μm. **B** Projected area of cells measured from images as shown in A. Sample size: Control = 1107, Evolved = 4281, $P = 1.387 * 10^2$. **C** Shape of cells measured as eccentricity from images as shown in A. Spherical cells have lower eccentricity. Sample size: Control = 1107, Evolved = 4281, P = 0. **D** Single cell mass density measured using a percoll gradient column. $P = 1.7867 * 10^7$. **E** Total biomass produced at stationary phase. $P = 1.1112 * 10^4$. **F** Fraction of cells budding in stationary phase measured from images as shown in A. Sample size: Control = 309, Evolved = 422, $P = 1.2079 * 10^6$. **G** Distribution of normalized fluorescence intensities of DNA in cells stained with SYTOX Green measured using flow cytometry. Sample size: Control = 199682, Evolved = 399113.

C. Freeze-thaw tolerant cells are smaller, denser and exhibit reduced budding

To investigate if there could be any morphological changes associated with the increased survival of cells, we imaged cells of the wild type yeast and the freeze-thaw tolerant yeast at stationary phase to measure their size (Figure 3**A**). We observed a two-fold reduction in cell area (Fig. 3**B**), which corresponds to an estimated six-fold volume reduction in freeze-tolerant cells. We also observed that freeze-thaw tolerant cells are more spherical in shape, compared to the ellipsoid shape of wild type cells, quantified by the eccentricity of cells (Fig. 3**C**). A decrease in volume of a cell could occur by decreased mass of a cell, increased density of a cell, or both. Measuring the single cell mass density of cells at stationary phase using a density gradient column, we find that the freeze-thaw tolerant cells had a significantly higher cell density (Fig. 3**D**). To estimate a change in mass of a single cell as a consequence of reduced volume and increased density, we measured the total biomass of the population at stationary phase. Although the total biomass produced by the evolved population is higher (Fig. 3**E**), the density increase is much lower compared to the six-fold cell volume reduction. Further, through estimation of the average mass of a cell from the total biomass and number of cells produced at stationary phase, we find that freeze-thaw tolerant cells have decreased total single cell mass on average. From the cellular morphologies, we also find a reduction in the incidence of budding in the evolved cell population (Fig. 3**F**), suggesting that they stopped doubling before reaching stationary phase and could have exited the cell cycle. This is also corroborated by a measurement of total amount of cellular DNA — the evolved cell population has reduced fraction of dual DNA copies (Fig. 3**G**).

The increased cellular mass density suggests that there could be an associated increase in the molecular crowding in the cytoplasm and thereby reduced cytoplasmic mobility and increased cellular stiffness. Since we also observed reduced membrane damage, next we investigated if the freeze-thaw tolerant cells are more mechanically resilient overall.

D. Freeze-thaw tolerant cells are mechanically stiffer

When yeast cells (ellipsoid) are exposed to Zymolyase, an enzyme mixture that digests the cell wall, spheroplasts are formed over time, which are spherical in shape (Fig. 4**A**). We imaged cells over the course of exposure to Zymolyase and measured their eccentricity over time. Figure 4**B** shows that freeze-thaw tolerant cells take much longer to turn spherical. However, a large fraction of the freeze-thaw tolerant cells did not turn spherical in the presence of Zymolyase even after a longer duration of time (Fig. 4**C,D**). The distribution of freeze-thaw sensitive cells (WT) shifts towards a lower eccentricity (more spherical) after 13 hours. Interestingly, the freeze-thaw tolerant cells have a distribution that shifts to the same eccentricity as that of the WT af-

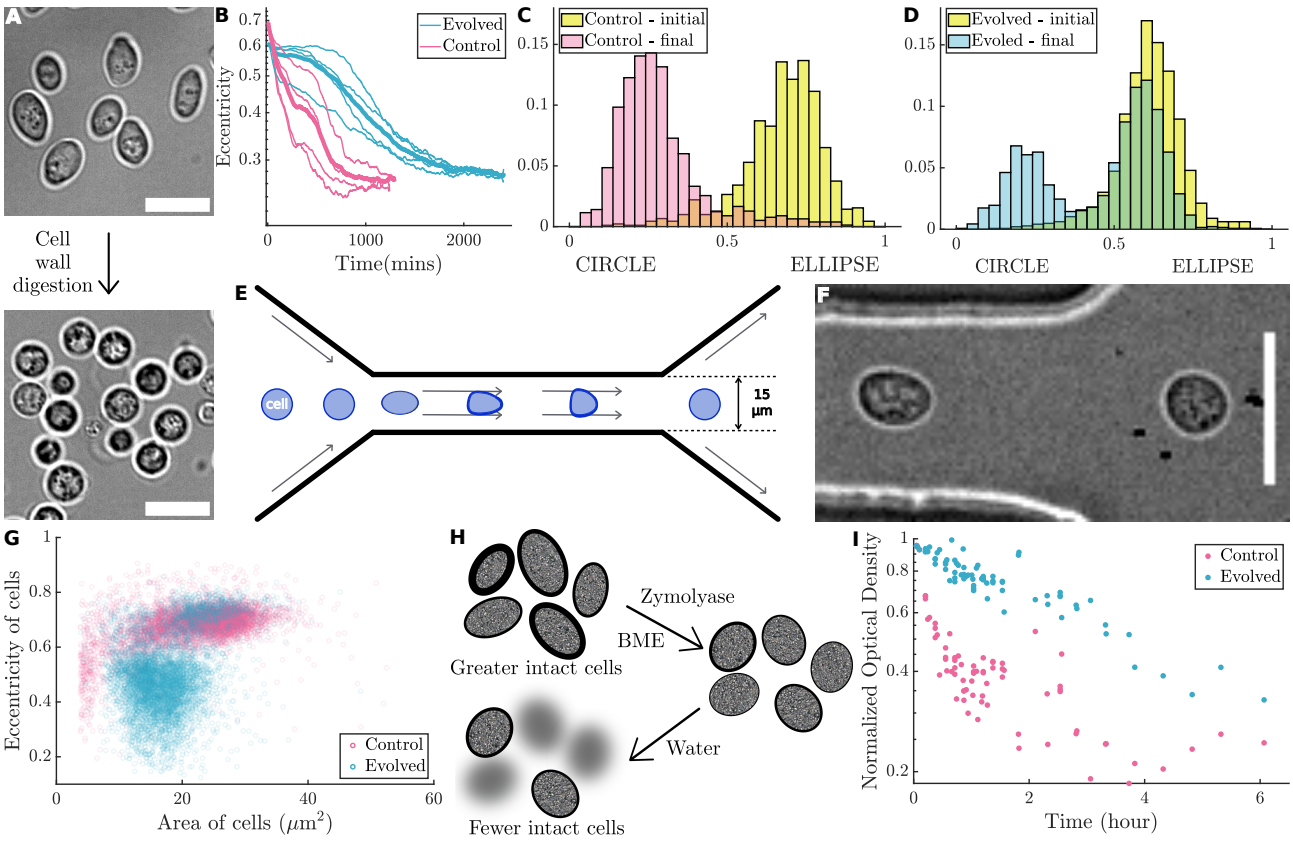

Figure 4. Population of cells adapted to freeze and thaw stress show differences in the ability of the cell to deform A Cell shape during enzymatic digestion of the cell wall. Scale bar - 10μm **B** Time-course of the mean eccentricity of the cells during enzymatic cell wall digestion. **C** Distributions of the initial and final eccentricities of the wild type population of cells during enzymatic cell wall digestion. **D** Distributions of the initial and final eccentricities of the evolved population of cells during enzymatic cell wall digestion. **E** Design of the microfluidic channel through which cells are flowed to measure deformation. **F** Image of cells leaving the microfluidic channel. Scale bar - 15μm **G** Eccentricity and area of cells measured in the narrow channel. Flow rate: Control - 5.5cm/s, Evolved - 5.6cm/s. **H** Sketch of the experimental design to probe the digestion of the cell wall. BME - beta-mercaptoethanol. **I** Fraction of intact cells over time measured by turbidity of cells placed in water after Zymolyase treatment.

ter 13 hours, but with a reduced peak height. Rather than a distribution of cells that shifts more slowly towards a spherical shape, we observed that a larger fraction of cells retained their shape even after a long duration of time. Munder *et al.* found that cells that had increased cytoplasmic stiffness did not relax after treatment with Zymolyase (20). Hence, the relaxation of cells from ellipsoidal to spherical could be affected either by their cytoplasmic stiffness or their cell wall resilience, due to a varied cell wall composition that is not affected by Zymolyase to the same extent. Therefore, to further investigate the role of these two factors, we performed deformability cytometry on cells exposed to Zymolyase, a method previously described by Otto *et al.* (34). Cells in a viscous buffer were pushed through a narrow microfluidic channel and the deformation of cells due to shear was measured as a function of their eccentricity (Fig. 4**E,F**). For a given cell size, lower cell stiffness results in a higher deformation and therefore higher eccentricity. We found two clusters of the freeze-thaw tolerant cells with a majority of cells minimally deformed, compared to the freeze-thaw sensitive (WT) cells (Fig. 4**G**). The presence of two clusters indicates that some cells could have retained their cell wall even after the long Zymolyase treatment.

In yeast, the cell wall maintains the structure of the cell. When the cell wall is removed and cells are placed in a hypo-osmotic environment, cells lyse as they cannot control the amount of water permeating into the cell. Therefore, to investigate the presence of the cell wall after digestion with Zymolyase, we exposed cells to Zymolyase for varying lengths of time in appropriate buffer followed by a hypo-osmotic environment *i.e.* pure water (Fig. 4**H**). Cells without their cell wall lyse when placed in water and we measured the turbidity of the solution as a measure of the fraction of intact cells. A significant fraction of the freeze-thaw tolerant cells do not lyse even after exposure to Zymolyase for long periods of time, compared to the duration taken for most of the freeze-thaw sensitive cells to lyse (Fig. 4*I*). This suggests three possibilities - (a) the freeze-thaw tolerant cells have an altered cell wall composition that is not easily digested by Zymolyase, (b) the cells have an altered membrane structure (as seen above) that does not allow water to enter the cell even after cell wall digestion, or (c) an increased cytoplasmic stiffness that does not allow cells to relax after cell wall digestion and hence the cellular components do not spread into solution enough to change the turbidity of the solution.

These results suggest that cells of the adapted popu-

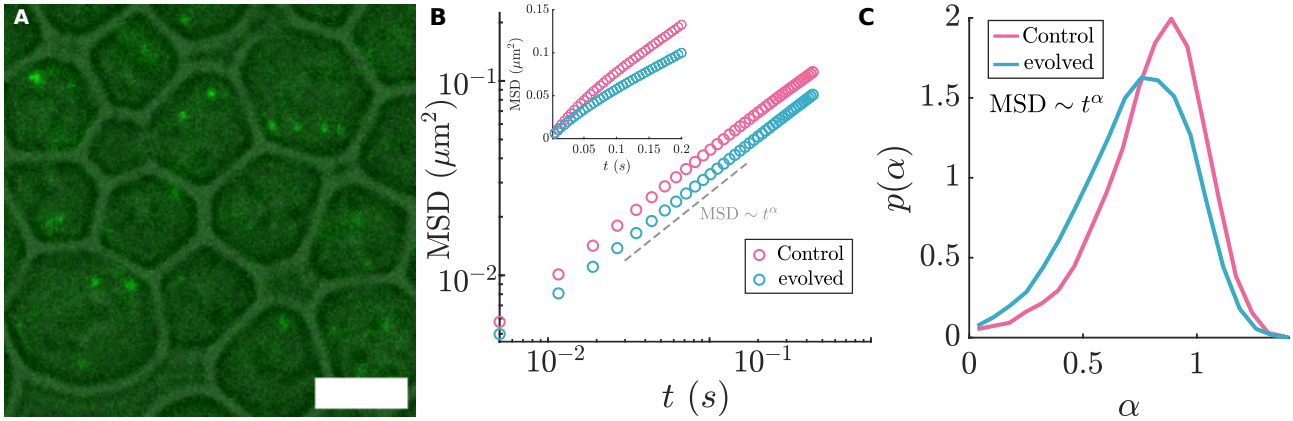

Figure 5. Population of cells adapted to freeze-thaw stress and refreezing stress exhibit cellular mechanical adaptations : decreased cytoplasmic fluidity A Image of Genetically Encoded Multimers (GEMs) in the cytoplasm of cells. Scale bar - 5μm. **B** Mean squared displacement (MSD) of GEMs tracked in the cytoplasm of cells, plotted on logarithmic axes. Inset: MSD plotted on linear axes. **C** Distribution of the exponent of time, α

lation have increased mechanical (structural) resilience associated with modified cell wall or cytoplasmic properties. We next specifically investigated the cytoplasmic rheology to understand the nature of the increased cellular stiffness.

E. Freeze-thaw tolerant cells exhibit reduced cytoplasmic mobility

To study the cytoplasmic mobility, we tracked the motion of engineered fluorescent particles (Fig. 5**A**). Freeze-thaw selection was performed on a strain that expressed fluorescent particles (41 nm diameter) that could be tracked in the cytoplasm. Briefly, to express these fluorescent particles, we transformed the wild type CEN.PK strain to express genetically encoded multimers (GEMs) using a plasmid developed by Delarue *et al.* (21). Delarue *et al.* replaced the INO4 promoter with the monomeric fluorophore sequence fused with the INO4 promoter and selected for the integrants using uracil auxotrophy. We inserted the monomeric fluorophore fused with the INO4 promoter at the HO locus in a prototroph which does not affect growth characteristics significantly in a diploid strain (35). The plasmid also contained a KanMX marker for selecting the integrants using resistance to G418. We imaged the GEMs expressed in the cell using total internal reflection fluorescence (TIRF) microscopy every 5 ms. We then tracked these particles and analysed the trajectories using custom written MATLAB code.

To quantify the mobility of these particles, we calculated the mean squared displacement (MSD) for several trajectories of many cells (using eq. S4). Two-dimensional MSD is related to the time window, t, in which it is calculated by $\mathrm{MSD}(t) \sim t^\alpha$, where the exponent, α, is related to the nature of motion of the particle. We calculated the MSD across all trajectories of all replicates, with each line on the plot representing an average of 10's of thousands of single particle trajectories. We found that the MSD is lower for particles in the cytoplasm of freeze-thaw tolerant cells (Fig. 5**B**). This suggests reduced mobility of particles in the cytoplasm of freeze-thaw tolerant cells. From the time and ensemble averaged MSD, we find $\alpha \approx 0.83$ for particles in the cytoplasm of freeze-thaw sensitive cells and $\alpha \approx 0.77$ for particles in the cytoplasm of freeze-thaw tolerant cells. The probability density function, $p(\alpha)$, of the exponent, calculated by fitting the time averaged MSD of a particle (calculated using eq. S2) to a power law, further reveals a larger fraction of particles exhibiting a significantly restricted motion in the freeze-thaw tolerant cells compared to the WT cells (Fig. 5**C**). We find this mechanical phenotype of decreased mobility and increased confinement of particles in the cytoplasm across all freeze-thaw adapted replicate lines.

F. Distinct genetic routes underlie the adaptations

Next, we performed whole genome sequencing to investigate if the increased cellular stiffness across all adapted populations is associated with a particular genotype (or specific genetic mutations). The starter culture, evolved strains, and control strains from the freeze-thaw evolution experiments were sequenced. The evolved and control population samples were collected from the middle and end of the evolution experiments to analyze the trajectory of mutation frequencies in the population (Fig. 6**A**). The DNA from cells of these populations was then isolated and sequenced on a NovaSeq 6000 platform.

The paired-end sequencing reads obtained were analyzed (Fig. 6**B-D** and Supplementary Information). Briefly, high-quality reads were filtered and mapped to a reference genome to find variants - single nucleotide polymorphisms (SNPs), insertions, and deletions. The true variants were initially filtered based on their alignment quality, total depth of coverage and fraction of reads supporting the variant. A 95% confidence interval of the frequency estimate was used to determine if there was a significant change in the variant frequency over the course of evolution, retaining only the variants with a minimum 20% frequency change in any sample (Fig. 6**C**).

If two or more variants are physically linked on the same

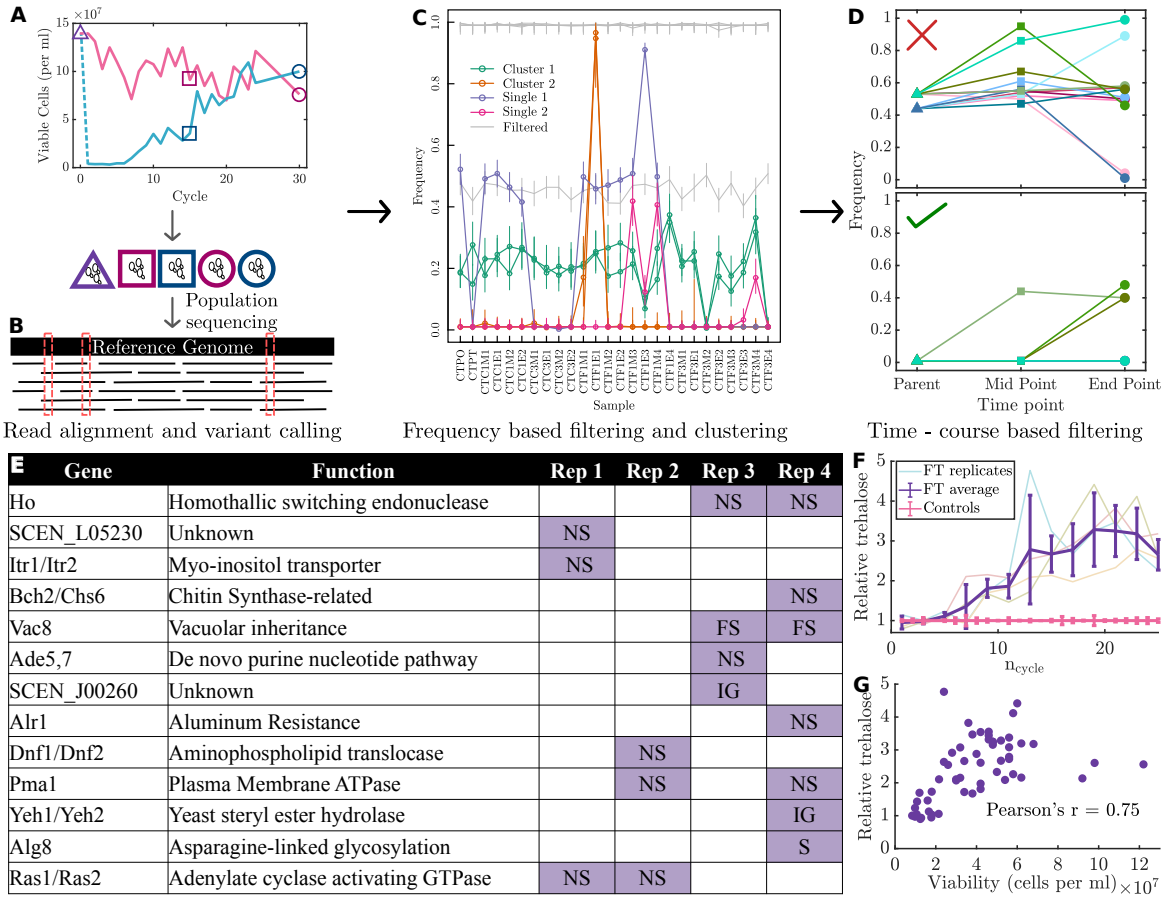

E

Gene	Function	Rep 1	Rep 2	Rep 3	Rep 4
Ho	Homothallic switching endonuclease			NS	NS
SCEN_L05230	Unknown	NS			
Itr1/Itr2	Myo-inositol transporter	NS			
Bch2/Chs6	Chitin Synthase-related				NS
Vac8	Vacuolar inheritance			FS	FS
Ade5,7	De novo purine nucleotide pathway			NS	
SCEN_J00260	Unknown			IG	
Alr1	Aluminum Resistance				NS
Dnf1/Dnf2	Aminophospholipid translocase		NS		
Pma1	Plasma Membrane ATPase		NS		NS
Yeh1/Yeh2	Yeast steryl ester hydrolase				IG
Alg8	Asparagine-linked glycosylation				S
Ras1/Ras2	Adenylate cyclase activating GTPase	NS	NS		

Figure 6. Replicates of populations of cells adapted to freeze-thaw stress do not have any specific genetic mutation in common A Representation of samples collected for sequencing. Sample collection points are displayed on a plot of the the number of viable cells in the control and evolving population across freeze-thaw-growth cycles. **B** Mapping of reads to a reference genome followed by variant calling. **C** A few representative variants filtered and clustered based on their frequency across all samples. Error bars denote 95% confidence intervals. **D** Trajectories of frequencies of representative variants from parent strain till the end point of selection. Each line represents a sample. **E** List of genetic mutations across all replicates. FS - Frame Shift, NS - Non-Synonymous, S - Synonymous, IG - Inter-genic region **F** Basal intracellular concentrations of trehalose relative to the control measured over the course of evolution. **G** Correlation of intracellular trehalose concentrations with viability after freeze-thaw measured over the course of evolution.

genome, their frequencies are expected to co-vary over time and across samples. Any such cluster of variants may contain only one adaptive driver among other background hitchhiking mutations. We identified potential drivers by clustering variants based on their frequencies across samples and selecting variants of the same gene that recurred across different clusters. Additionally, variants associated with increased fitness are expected to show the same directional change in frequency over time and across samples. Hence, the trajectories of variant frequencies were analysed over the course of evolution for each sample, from parent to mid-point till end point, and only those variants with a monotonic change in frequency across time and samples were retained.

The final list of all variants obtained for the freeze-thaw tolerant populations, along with their function are shown in Fig. 6**E**. For each variant, the samples in which it was found is marked and labeled by the nature of the mutation. We then checked if there were any variants that were present across multiple samples as this would implicate that the mechanical phenotype found across all replicates was a consequence of a specific genotype(s). We find that there are no variants common across all replicates. This suggests that the mechanical phenotype found is a result of distinct genetic routes and there is no specific genotype associated with the mechanical phenotype of increased cellular stiffness. Since we do not find any specific genotype responsible for the altered phenotype, we probed the molecular composition of the cell to understand if the increased cellular stiffness could be due to an altered molecular composition.

G. Evolved cells have higher basal intracellular levels of trehalose

Trehalose is a sugar containing two α-glucose units with a 1,1-glycosidic bond between them. Several studies have found a strong correlation between intracellular trehalose concentration and survival after freeze-thaw (36; 37). Chen *et al.* showed that trehalose was sufficient to confer freeze-thaw tolerance when cooled slowly to -80°C (9). These studies either measure the amount of trehalose in existing freeze-thaw tolerant strains or the survival in trehalose accumulated mutant strains. We investigated if increased trehalose concentration could emerge as an adaptation to freeze-thaw stress. We measured the amounts of intracellular tre-

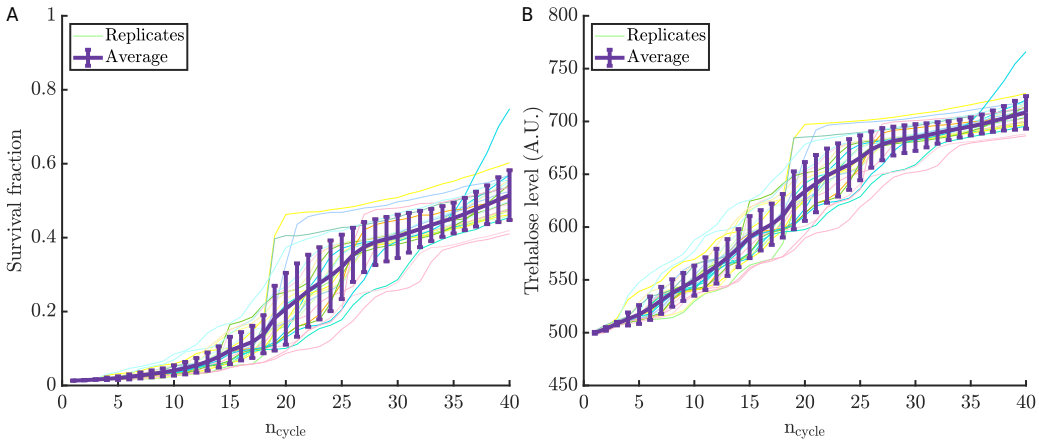

Figure 7. Simulated adaptation of yeast to freeze-thaw based on a trehalose linked entry into a quiescence like state resembles the results of experimental evolution of yeast to freeze-thaw A Survival fraction of cells after freeze-thaw over the course of evolution. **B** Basal intracellular concentrations of trehalose relative to the control over the course of evolution.

halose at the stationary phase to calculate the basal levels of trehalose present in cells, over the course of adaptation to freeze-thaw. Cell colonies were collected and weighed from plates used to measure survival using CFUs 48 hours after thawing. The concentration of trehalose was then measured using a previously described protocol (14). Cells were lysed and glucose present in cells was broken down. The trehalose present was then converted to glucose using Trehalase and the concentration of glucose was measured using a colorimetric assay. We find that the amount of basal intracellular trehalose increases over the course of adaptation to freeze-thaw (Fig. 6**F**). As also seen from the time course of the increase in cell survival (Fig. 1**B**), this increase in trehalose highly correlated with cell viability after freeze-thaw (Fig. 7**G**).

Interestingly, our sequencing analysis did not reveal any mutations directly related to trehalose synthesis, degradation or transport (Fig. 6). Therefore, this increased concentration of trehalose is not of any direct genetic origin, unlike previous studies that used trehalose synthesis, degradation or transport mutants and related viability after freeze-thaw to trehalose concentration (9; 36; 37).

These findings of increased intracellular trehalose also correlate with reduced membrane damage and increased cytoplasmic stiffness. Using trehalose synthesis, degradation or transport mutants, trehalose has been previously found to protect membranes during desiccation and freezing (38; 39; 40) and to alter the cytoplasmic fluidity during temperature stress (23). Although several other factors may be involved in increased membrane resilience and decreased cytoplasmic fluidity, our study finds a relation between increased trehalose, reduced membrane damage and decreased cytoplasmic fluidity that emerged as a result of evolutionary adaptation to freeze-thaw stress.

H. Selection based on a trehalose linked entry into a quiescence-like state recapitulates the adaptation dynamics

Increased intracellular trehalose is a defining characteristic of quiescent cells (41). Quiescent cells have been found to be denser due to the presence of trehalose, increased cell wall thickness and reduction in cell volume (29). Quiescent cells have also been found to be associated with a decreased cytoplasmic fluidity (42). Coincidentally, all these attributes associated with quiescent cells are characteristics we found in freeze-thaw adapted cells. Although all cells enter a non-dividing state upon nutrient starvation, quiescent cells have better ability to survive stress and rapidly fluctuating environments and re-enter the cell cycle once conditions are favourable (43; 13). Therefore, we simulate the adaptation of yeast based on the ability of cells to enter and exit quiescence (full details in Supplementary Information). Briefly, we use a population level simulation with trehalose concentration acting as the sole phenotype under selection (41). We start with an initial population with its phenotypic trehalose distribution drawn from a Gaussian distribution. We assume that the trehalose level for each cell in stationary phase is correlated with its growth rate in log phase (44; 45), and directly determines (a) the probability of going into a quiescent state upon encountering starvation conditions (46; 47), (b) the probability of survival after freeze thaw (28; 48; 49; 16; 50), and (c) the duration of lag phase upon re-entry into the cell cycle (43; 51; 52; 53).
In each cycle of growth-freeze-thaw, the population has differing growth rates, and cells with lower trehalose values have a higher growth rate and a larger number of offspring. Each offspring is allowed a small mutation which acts to shift its stationary state trehalose concentration with respect to its parent. These mutational effects are drawn from a fat-tailed distribution symmetric about zero *i.e.* most mutations have no effect on the phenotype of the offspring, while the possibility of a few large effect mutations exists. Each cell division uses up a unit of a finite resource, and the population faces star-

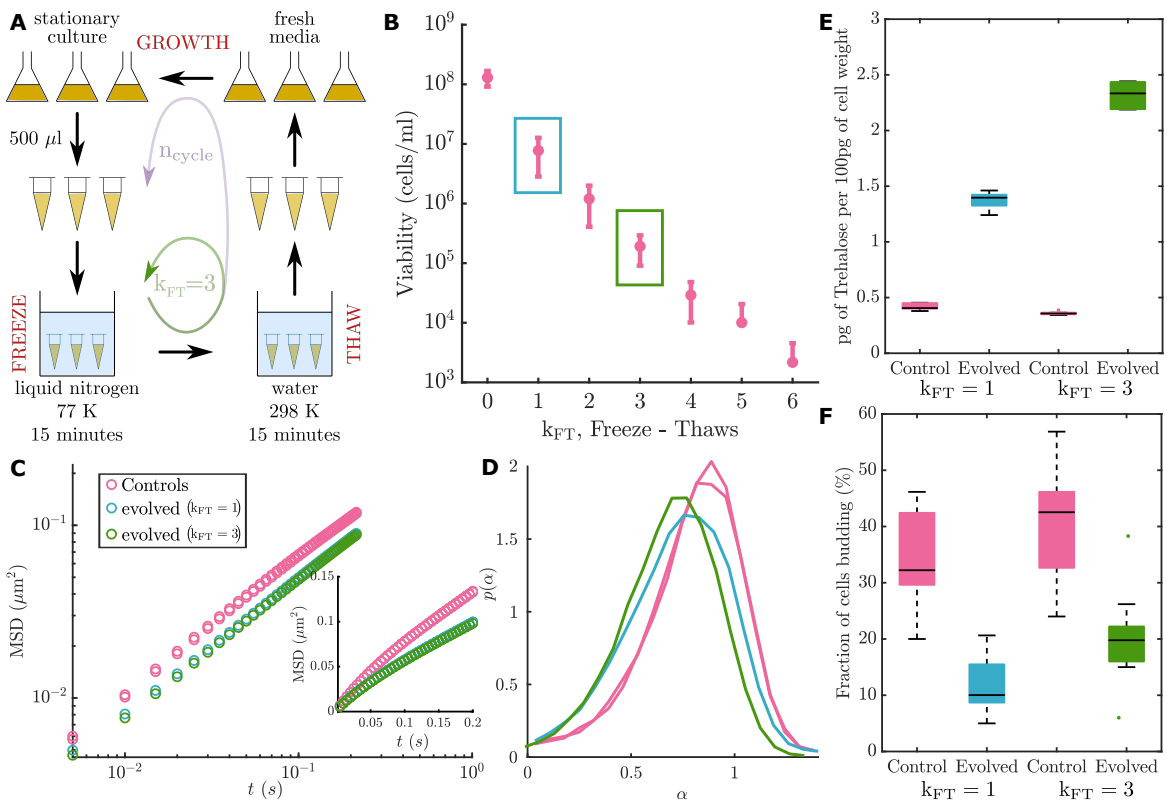

Figure 8. Convergent mechano-chemical adaptation to freeze-thaw A Experimental design to measure survival after refreezing and for the evolution of refreezing tolerance. **B** Number of viable cells after consecutive freeze-thaws. **C** Mean squared displacement (MSD) of GEMs tracked in the cytoplasm of cells, plotted on logarithmic axes. Inset: MSD plotted on linear axes. **D** Distribution of the exponent of time, α. **E** Basal amounts of intracellular trehalose measured in the stationary phase. $P(k_{FT}=1) = 9.132*10^{11}$, $P(k_{FT}=3) = 3.6926*10^{12}$. **F** Fraction of cells budding measured in the stationary phase. Sample size: Control ($k_{FT}=1$) = 309, Evolved ($k_{FT}=1$) = 422, $P(k_{FT}=1) = 1.2079*10^{6}$, Control ($k_{FT}=3$) = 357, Evolved ($k_{FT}=3$) = 459, $P(k_{FT}=3) = 7.5733*10^{5}$.

vation when the resource runs out.

Upon starvation, the population differentiates into quiescent and non-quiescent cells. Cells with higher amounts of trehalose have a higher probability of entering a quiescent state. All non-quiescent cells are subsequently assumed to perish when the population is subjected to selection *i.e.* freeze-thaw. The survival of cells after freeze thaw is determined similarly, using a survival probability that increases with the intracellular trehalose concentration. The population that survives freeze-thaw is diluted by selecting a fraction of the population randomly, which is then allowed to enter growth again. The lag phase of each cell is further determined by its trehalose concentration, with cells with higher trehalose concentrations facing a shorter lag time.

Thus, the states of quiescence and increased survival under freeze thaw cause the population distribution to shift to higher values of mean trehalose. Similarly, cells with higher trehalose have longer periods of growth due to a shorter lag phase, and take over more of the population with each generation of offspring. This effect is diminished slightly by the fact that higher trehalose also leads to a smaller growth rate, but is not strong enough initially to stall the increase in mean trehalose of the population. At larger values of trehalose the effect of a decreasing growth rate becomes stronger, leading to saturation of trehalose levels over the course of evolution. We find that when cells are selected in this way for quiescence, the survival and trehalose levels of the adapting population qualitatively resembles the survival (Fig. 7**A**) and trehalose levels (Fig. 7**B**) of the freeze-thaw adapting population. We see more sudden jumps in the experimental curves since the number of replicates in our experimental system is fewer than what the simulation allows for. Altogether, our results suggest that cellular entry into a quiescence-like state facilitates the adaptation to freeze-thaw.

I. The mechano-chemical adaptation is convergent

Finally, we ask if the results we describe thus far are a result of the specific selection protocol we used for experimental evolution or if they point to a more general mechanism. Therefore, we sought to investigate the phenotypes emerging from a different freeze-thaw selection regime.

To do this, we developed a selection protocol based on exposing cells to multiple consecutive freeze-thaw cycles before a growth cycle (Fig. 8**A**). First, we note that the survival fraction of the cells decreases exponentially with consecutive free-thaw exposures, reducing by about an order of magnitude with the number of consecutive exposures, k_{FT} (Fig. 8**B**). Each point obtained by varying k_{FT} is therefore a quantitatively (and qualitatively) different selection regime. Although the results obtained so far have been obtained from the $k_{FT}=1$ regime, we now report results from the $k_{FT}=3$ selec-

tion regime. Interestingly, despite a nearly two orders of magnitude reduction in viability, the yeast adapted to the $\mathrm{k_{FT}} = 3$ regime, with survival close to 40%. The MSDs obtained from cells of the evolved population in the $\mathrm{k_{FT}} = 3$ regime fall directly on top of those obtained from the $\mathrm{k_{FT}} = 1$ regime (Fig. 8**B**); the distribution of the MSD exponents, $p(\alpha)$ is also quite similar (Fig. 8**C**).

Furthermore, we find that the population of cells evolved in this regime also exhibits a multifold increase in basal trehalose levels (Fig. 8**E**) and reduced budding fractions (Fig. 8**F**). We also do not find any unique, common genetic modifications in the adaptation outcomes of the $\mathrm{k_{FT}} = 3$ selection regime (Fig. S4). On the basis of these findings, we conclude that the mechano-chemical phenotype promoting cellular entry into a quiescence-like state is a convergent adaptation.

Discussion

Using experimental evolution, we have shown that *Saccharomyces cerevisiae* can adapt to high freeze rate perturbations in a stereotypical manner, with survival increasing nearly two orders of magnitude over 25 cycles of freeze-thaw-growth. The adapted cells exhibit smaller sizes, higher mass densities, and reduced membrane damage. Using rheological measurements we showed that the adapted cells are stiffer and exhibited lower particle mobility within the cytoplasm. Whole genome sequencing indicated that the increased survival is associated with multiple, distinct genotypes. Despite the lack of a singular genetic cause, in all our replicate lines of evolution, the basal intracellular level of trehalose, a sugar speculated to play a physical role in maintaining membrane and cytoplasmic integrity (17; 54; 23), exhibited a drastic increase in the adapted cells. To our knowledge, this is the first study showing the *de novo* linkage between increased intracellular trehalose, reduced membrane damage, decreased cytoplasmic mobility and increased cellular stiffness.

The high levels of trehalose could play multiple roles in the increased mechanical resilience of the cell. Reduced membrane damage in freeze-thaw tolerant cells could be a result of altered lipid composition, altered cell wall composition and increased trehalose. Several studies show that increased membrane fluidity of cells was associated with higher freeze-thaw tolerance, with trehalose hypothesized to aid in membrane fluidization (30; 26; 25). In addition, our results on the increased cellular stiffness suggest that the cell wall composition could also be altered, thereby protecting the cell wall associated membrane from undergoing damage.

A major cause of death after freeze-thaw has been suggested to be ice crystal formation (55; 4; 56; 17). Ice crystals can damage the cell membrane, proteins in the cytoplasm and disrupt the intracellular structure and organisation, thereby hindering the revival of cellular processes upon thawing. A glassy cytoplasm with decreased mobility is a cytoplasmic rheological state that could aid in retaining cellular structure and organisation during freeze-thaw transitions. Indeed such a cytoplasmic state has been implicated in response to various environmental stresses (19; 20; 21; 23) and has also long been associated with freeze-thaw tolerance. We found the *de novo* encoding of a similar cytoplasmic state in the adapted freeze-thaw tolerant cells.

Trehalose has been shown to be a good glass-former, compared to other sugars like glucose and sucrose (57) and has also been found to localise in the cytosol (50). Several other studies showed that higher intracellular trehalose levels are associated with tolerance to desiccation, heat, ethanol etc (13; 58). Cakar *et al.* allowed mutagenic lines of *Saccharomyces cerevisiae* to adapt to various kinds of stresses and found that freeze-thaw tolerant populations were tolerant to multiple other kinds of stress such as high temperature, ethanol and oxidative stress (59). Since the freeze-thaw tolerant cells were found to have decreased cytoplasmic fluidity and increased intracellular trehalose, together, it suggests that mechanical adaptations could facilitate survival of cells in various kinds of environmental stresses. In addition, our findings of the lack of common genetic mutations across freeze-thaw or refreezing tolerant populations strengthen the idea that selection occurred based on the mechanical phenotype of cells rather than other phenotypes dependent on specific molecules or molecular pathways. As the increased trehalose levels were not found to have any direct genetic association, we hypothesize that the levels of trehalose could also be regulated by the cell indirectly through various different pathways (apart from the direct synthesis, degradation or transport pathways) in response to environmental stress.

While freeze-thaw is lethal to most kinds of cells, several cells survive freeze-thaw on ecological and evolutionary timescales. There have been a few previous studies that used experimental evolution to obtain freeze-thaw tolerance in cells. Kwon *et al.* started with a *L. rhamnosus* strain that had a 60% survival fraction after freeze-thaw and the adapted strain was found to have a $\approx$1.5 fold increase in survival fraction over 150 freeze-thaw-growth cycles (26). Sleight *et al.* found only a 2.5 times increase in survival fraction of *E. coli* over 150 freeze-thaw-growth cycles (1000 generations) (25). Although, these studies are on very different species, they both find *cls* mutants that increase membrane fluidity to be associated with survival. Since these kinds of stress do not cause a drastic reduction in survival, it could lead to a more gradual phenotypic change as fitness is not affected as much – it must be noted that in our experiments, the survival of wild type *Saccharomyces cerevisiae* to rapid freeze-thaw is a few percent or lesser. By using freeze-thaw regimes where survival is affected significantly, we found that *Saccharomyces cerevisiae* adapts to have orders of magnitude higher survival in only $\approx$25 freeze-thaw-growth cycles

(≈100 generations). Our observations of stark phenotypic changes could be because of the strong selection regime in which we operate.

The various cellular attributes that we have discovered in our study correlate with those of quiescent cells. The molecular mechanisms of quiescence entry and exit and the characteristics of the quiescent state have only recently been understood (43; 29) — specifically, trehalose promotes efficient entry into and exit from quiescence. Our simulations on trehalose-mediated selection for quiescence suggest that an entry to a quiescence-like state, as well as the ease of re-entering the growth cycle (through lag) facilitates the adaptation dynamics we see in the experiments.

Several studies have found that quiescent cells are more stress resilient (60), although the underlying mechanisms underlying have not yet been understood. Genes involved in the stress response leading to quiescence have been studied through enrichment of quiescent cells in the population (61) but these genetic mutations are not present among the adapted populations in our experiments. The emergence of a quiescence-like state in our experimental evolution study, suggests that increased mechanical resilience of a quiescent cell could be responsible for stress resilience.

Finally, we found similar mechano-chemical adaptations not only across replicate evolution lines but also across different selection regimes — altogether, a convergent physical adaptation to a quiescence-like state can facilitate stress response in yeast.

Acknowledgments

We thank Sunil Laxman and Stephan Herminghaus for help and discussions with the project. We acknowledge support from the Department of Atomic Energy (India), under project no. RTI4006, and the Simons Foundation (Grant No. 287975). We acknowledge funding from the Human Frontier Science Program and the Max Planck Society through a Max-Planck-Partner-Group. We thank the Central Imaging and Flow Cytometry Facility, Sequencing Facility and computational facility at NCBS. The authors also thank the Sane lab at NCBS for access to a high speed camera and the Mayor lab at NCBS for access to TIRF microscopy.

1. Peter Mazur and Janice J Schmidt. Interactions of cooling velocity, temperature, and warming velocity on the survival of frozen and thawed yeast. *Cryobiology*, 5(1):1–17, 7 1968. URL: https://linkinghub.elsevier.com/retrieve/pii/S0011224068801385http://www.ncbi.nlm.nih.gov/pubmed/5760041, doi:10.1016/s0011-2240(68)80138-5.
2. S P Leibo, John Farrant, Peter Mazur, M G Hanna, and L.H. H Smith. Effects of freezing on marrow stem cell suspensions: interactions of cooling and warming rates in the presence of PVP, sucrose, or glycerol. *Cryobiology*, 6(4):315–32, 1 1970. URL: https://linkinghub.elsevier.com/retrieve/pii/S0011224070800864http://www.ncbi.nlm.nih.gov/pubmed/4192533, doi:10.1016/s0011-2240(70)80086-4.
3. Hans Ramløv and Peter Westh. Survival of the cryptobiotic eutardigrade Adorybiotus coronifer during cooling to -196 °C: Effect of cooling rate, trehalose level, and short-term acclimation. *Cryobiology*, 29(1):125–130, 1992. doi:10.1016/0011-2240(92)90012-Q.
4. P. Mazur. Freezing of living cells: mechanisms and implications. *American Journal of Physiology-Cell Physiology*, 247(3):C125–C142, 9 1984. URL: http://ajpcell.physiology.org/http://ajpcell.physiology.org/content/247/3/C125https://journals.physiology.org/doi/10.1152/ajpcell.1984.247.3.C125, doi:10.1152/ajpcell.1984.247.3.C125.
5. Sonia Rodriguez-Vargas, Francisco Estruch, and Francisca Randez-Gil. Gene expression analysis of cold and freeze stress in Baker's yeast. *Applied and Environmental Microbiology*, 68(6):3024–3030, 2002. doi:10.1128/AEM.68.6.3024-3030.2002.
6. A. Pacheco, C. Pereira, M. J. Almeida, and M. J. Sousa. Small heat-shock protein Hsp12 contributes to yeast tolerance to freezing stress. *Microbiology*, 155(6):2021–2028, 2009. doi:10.1099/mic.0.025981-0.
7. Maria M. Bayliak, Olha V. Hrynkiv, Roksolana V. Knyhynytska, and Volodymyr I. Lushchak. Alpha-ketoglutarate enhances freeze–thaw tolerance and prevents carbohydrate-induced cell death of the yeast Saccharomyces cerevisiae. *Archives of Microbiology*, pages 1–14, 2017. doi:10.1007/s00203-017-1423-9.
8. Olga Kandror, Nancy Bretschneider, Evgeniy Kreydin, Duccio Cavalieri, and Alfred L. Goldberg. Yeast Adapt to Near-Freezing Temperatures by STRE/Msn2,4-Dependent Induction of Trehalose Synthesis and Certain Molecular Chaperones. *Molecular Cell*, 13(6):771–781, 3 2004. URL: http://linkinghub.elsevier.com/retrieve/pii/S1097276504001480https://linkinghub.elsevier.com/retrieve/pii/S1097276504001480, doi:10.1016/S1097-2765(04)00148-0.
9. Anqi Chen and Patrick A. Gibney. Intracellular trehalose accumulation via the Agt1 transporter promotes freeze–thaw tolerance in Saccharomyces cerevisiae. *Journal of Applied Microbiology*, 133(4):2390–2402, 10 2022. URL: https://academic.oup.com/jambio/article/133/4/2390/6989000, doi:10.1111/jam.15700.
10. Gaber Zayed and Yrjo H. Roos. Influence of trehalose and moisture content on survival of Lactobacillus salivarius subjected to freeze-drying and storage. *Process Biochemistry*, 39(9):1081–1086, 5 2004. URL: https://linkinghub.elsevier.com/retrieve/pii/S003295920300222X, doi:10.1016/S0032-9592(03)00222-X.
11. Jon P. Costanzo, Richard E. Lee, and Peter H. Lortz. Glucose Concentration Regulates Freeze Tolerance In the Wood Frog Rana Sylvatica. *Journal of Experimental Biology*, 181(1):245–255, 8 1993. URL: https://journals.biologists.com/jeb/article/181/1/245/6632/Glucose-Concentration-Regulates-Freeze-Tolerance, doi:10.1242/jeb.181.1.245.
12. Thomas C. Boothby, Hugo Tapia, Alexandra H. Brozena, Samantha Piszkiewicz, Austin E. Smith, Ilaria Giovannini, Lorena Rebecchi, Gary J. Pielak, Doug Koshland, and Bob Goldstein. Tardigrades Use Intrinsically Disordered Proteins to Survive Desiccation. *Molecular Cell*, 65(6):975–984, 3 2017. doi:10.1016/j.molcel.2017.02.018.
13. Hugo Tapia, Lindsey Young, Douglas Fox, Carolyn R. Bertozzi, and Douglas Koshland. Increasing intracellular trehalose is sufficient to confer desiccation tolerance to Saccharomyces cerevisiae. *Proceedings of the National Academy of Sciences*, 112(19):6122–6127, 5 2015. URL: http://www.ncbi.nlm.nih.gov/pubmed/25918381http://www.pnas.org/lookup/doi/10.1073/pnas.1506415112http://www.pubmedcentral.nih.gov/articlerender.fcgi?artid=PMC4434740https://pnas.org/doi/full/10.1073/pnas.1506415112, doi:10.1073/pnas.1506415112.
14. Cihan Erkut, Vamshidhar R Gade, Sunil Laxman, and Teymuras V Kurzchalia. The glyoxylate shunt is essential for desiccation tolerance in C. elegans and budding yeast. *eLife*, 5:1–24, 4 2016. URL: http://elifesciences.org/lookup/doi/10.7554/eLife.13614https://elifesciences.org/articles/13614, doi:10.7554/eLife.13614.
15. Steffen Hengherr, Arnd G. Heyer, Heinz R. Köhler, and Ralph O. Schill. Trehalose and anhydrobiosis in tardigrades - Evidence for divergence in responses to dehydration. *FEBS Journal*, 275(2):281–288, 2008. doi:10.1111/j.1742-4658.2007.06198.x.
16. Juan Carlos Argüelles. Physiological roles of trehalose in bacteria and yeasts: a comparative analysis. *Archives of Microbiology*, 174(4):217–224, 9 2000. URL: http://link.springer.com/10.1007/s002030000192http://www.ncbi.nlm.nih.gov/pubmed/11081789, doi:10.1007/s002030000192.
17. Samuel B Leslie, Eitan Israeli, Bruce Lighthart, J. H. Crowe, and Lois M Crowe. Trehalose and sucrose protect both membranes and proteins in intact bacteria during drying. *Applied and Environmental Microbiology*, 61(10):3592–3597, 10 1995. URL: http://aem.asm.org/http://www.ncbi.nlm.nih.gov/pubmed/7486995http://www.pubmedcentral.nih.gov/articlerender.fcgi?artid=PMC167656https://journals.asm.org/doi/10.1128/aem.61.10.3592-3597.1995, doi:10.1128/aem.61.10.3592-3597.1995.
18. Roberto D. Lins, Cristina S. Pereira, and Philippe H. Hünenberger. Trehalose-Protein Interaction in Aqueous Solution. *Proteins: Structure, Function and Genetics*, 55(1):177–186, 2004. doi:10.1002/prot.10632.
19. Bradley R. Parry, Ivan V. Surovtsev, Matthew T. Cabeen, Corey S. O'Hern, Eric R. Dufresne, and Christine Jacobs-Wagner. The Bacterial Cytoplasm Has Glass-like Properties and Is Fluidized by Metabolic Activity. *Cell*, 156(1-2):183–194, 1 2014. URL: http://dx.doi.org/10.1016/j.cell.2013.11.028https://linkinghub.elsevier.com/retrieve/pii/S0092867413014797http://www.ncbi.nlm.nih.gov/pubmed/24361104http://www.pubmedcentral.nih.gov/articlerender.fcgi?artid=PMC3956598, doi:10.1016/j.cell.2013.11.028.
20. Matthias Christoph Munder, Daniel Midtvedt, Titus Franzmann, Elisabeth Nuske, Oliver Otto, Maik Herbig, Elke Ulbricht, Paul Müller, Anna Taubenberger, Shovamayee Maharana, Liliana Malinovska, Doris Richter, Jochen Guck, Vasily Zaburdaev, and Simon Alberti. A pH-driven transition of the cytoplasm from a fluid- to a solid-like state promotes entry into dormancy. *eLife*, 5:e09347, 3 2016. URL: https://elifesciences.org/articles/09347, doi:10.7554/eLife.09347.
21. M. Delarue, G.P. Brittingham, S. Pfeffer, I.V. Surovtsev, S. Pinglay, K.J. Kennedy, M. Schaffer, J.I. Gutierrez, D. Sang, G. Poterewicz, J.K. Chung, J.M. Plitzko, J.T. Groves, C. Jacobs-Wagner, B.D. Engel, and L.J. Holt. mTORC1 Controls Phase Separation and the Biophysical Properties of the Cytoplasm by Tuning Crowding. *Cell*, 174(2):338–349, 7 2018. URL: https://linkinghub.elsevier.com/retrieve/pii/S0092867418306548, doi:10.1016/j.cell.2018.05.042.
22. Joseph L. Watson, Estere Seinkmane, Christine T. Styles, Andrei Mihut, Lara K. Krüger, Kerrie E. McNally, Vicente Jose Planelles-Herrero, Michal Dudek, Patrick M. McCall, Silvia Barbiero, Michael Vanden Oever, Sew Yeu Peak-Chew, Benjamin T.

Porebski, Aiwei Zeng, Nina M. Rzechorzek, David C. S. Wong, Andrew D. Beale, Alessandra Stangherlin, Margot Riggi, Janet Iwasa, Jörg Morf, Christos Miliotis, Alina Guna, Alison J. Inglis, Jan Brugués, Rebecca M. Voorhees, Joseph E. Chambers, Qing-Jun Meng, John S O'Neill, Rachel S. Edgar, and Emmanuel Derivery. Macromolecular condensation buffers intracellular water potential. *Nature*, 623(7988):842–852, 11 2023. URL: https://www.nature.com/articles/s41586-023-06626-zhttp://www.ncbi.nlm.nih.gov/pubmed/37853127http://www.pubmedcentral.nih.gov/articlerender.fcgi?artid=PMC10665201, doi:10.1038/s41586-023-06626-z.

23. Laura B. Persson, Vardhaan S. Ambati, and Onn Brandman. Cellular Control of Viscosity Counters Changes in Temperature and Energy Availability. *Cell*, 183(6):1572–1585, 12 2020. URL: https://linkinghub.elsevier.com/retrieve/pii/S0092867420313805, doi:10.1016/j.cell.2020.10.017.
24. E H Zhou, X Trepat, C Y Park, G Lenormand, M N Oliver, S M Mijailovich, C Hardin, D A Weitz, J P Butler, and J J Fredberg. Universal behavior of the osmotically compressed cell and its analogy to the colloidal glass transition. *Proceedings of the National Academy of Sciences*, 106(26):10632–10637, 6 2009. URL: http://www.pubmedcentral.nih.gov/articlerender.fcgi?artid=2695406&tool=pmcentrez&rendertype=abstracthttps://pnas.org/doi/full/10.1073/pnas.0901462106, doi:10.1073/pnas.0901462106.
25. Sean C Sleight, Christian Orlic, Dominique Schneider, and Richard E Lenski. Genetic basis of evolutionary adaptation by Escherichia coli to stressful cycles of freezing, thawing and growth. *Genetics*, 180(1):431–43, 9 2008. URL: http://www.ncbi.nlm.nih.gov/pubmed/18757947http://www.pubmedcentral.nih.gov/articlerender.fcgi?artid=PMC2535694, doi:10.1534/genetics.108.091330.
26. Ye Won Kwon, Jae-Han Bae, Seul-Ah Kim, and Nam Soo Han. Development of Freeze-Thaw Tolerant Lactobacillus rhamnosus GG by Adaptive Laboratory Evolution. *Frontiers in Microbiology*, 9(NOV):1–10, 11 2018. URL: https://www.frontiersin.org/article/10.3389/fmicb.2018.02781/full, doi:10.3389/fmicb.2018.02781.
27. Akihiro Hino, Kohji Mihara, Kohtaro Nakashima, and H. Takano. Trehalose levels and survival ratio of freeze-tolerant versus freeze-sensitive yeasts. *Applied and environmental microbiology*, 56(5):1386–91, 5 1990. URL: http://aem.asm.org/http://www.ncbi.nlm.nih.gov/pubmed/2339891http://www.pubmedcentral.nih.gov/articlerender.fcgi?artid=PMC184415, doi:10.1128/aem.56.5.1386-1391.1990.
28. L. Diniz-Mendes, E. Bernardes, P. S. de Araujo, A. D. Panek, and V. M. F. Paschoalin. Preservation of frozen yeast cells by trehalose. *Biotechnology and Bioengineering*, 65(5):572–578, 12 1999. URL: https://onlinelibrary.wiley.com/doi/10.1002/(SICI)1097-0290(19991205)65:5%3C572::AID-BIT10%3E3.0.CO;2-7, doi:10.1002/(SICI)1097-0290(19991205)65:5<572::AID-BIT10>3.0.CO;2-7.
29. Siyu Sun and David Gresham. Cellular quiescence in budding yeast. *Yeast (Chichester, England)*, 38(1):12–29, 1 2021. URL: https://onlinelibrary.wiley.com/doi/10.1002/yea.3545http://www.ncbi.nlm.nih.gov/pubmed/33350503http://www.pubmedcentral.nih.gov/articlerender.fcgi?artid=PMC8208048, doi:10.1002/yea.3545.
30. J. Kruuv, J.R. Lepock, and A.D. Keith. The effect of fluidity of membrane lipids on freeze-thaw survival of yeast. *Cryobiology*, 15(1):73–79, 2 1978. URL: https://linkinghub.elsevier.com/retrieve/pii/0011224078900093, doi:10.1016/0011-2240(78)90009-3.
31. Yuhui Li, Hao Wang, and Pan Tingrui. Intracellular ice formation (IIF) during freeze-thaw repetitions. *International Journal of Heat and Mass Transfer*, 64:436–443, 2013. URL: http://dx.doi.org/10.1016/j.ijheatmasstransfer.2013.04.036, doi:10.1016/j.ijheatmasstransfer.2013.04.036.
32. P. H. Calcott and R. A. MacLeod. The survival of Escherichia coli from freeze–thaw damage: the relative importance of wall and membrane damage. *Canadian Journal of Microbiology*, 21(12):1960–1968, 12 1975. URL: http://www.nrcresearchpress.com/doi/10.1139/m75-284, doi:10.1139/m75-284.
33. Isabelle Sagot and Damien Laporte. The cell biology of quiescent yeast – a diversity of individual scenarios. *Journal of Cell Science*, 132(1), 1 2019. URL: https://journals.biologists.com/jcs/article/132/1/jcs213025/3037/The-cell-biology-of-quiescent-yeast-a-diversity-of, doi:10.1242/jcs.213025.
34. Oliver Otto, Philipp Rosendahl, Alexander Mietke, Stefan Golfier, Christoph Herold, Daniel Klaue, Salvatore Girardo, Stefano Pagliara, Andrew Ekpenyong, Angela Jacobi, Manja Wobus, Nicole Töpfner, Ulrich F. Keyser, Jörg Mansfeld, Elisabeth Fischer-Friedrich, and Jochen Guck. Real-time deformability cytometry: on-the-fly cell mechanical phenotyping. *Nature methods*, 12(3):199–202, 3 2015. URL: http://www.ncbi.nlm.nih.gov/pubmed/25643151, doi:10.1038/nmeth.3281.
35. W. P. Voth. Yeast vectors for integration at the HO locus. *Nucleic Acids Research*, 29(12):59e–59, 2002. doi:10.1093/nar/29.12.e59.
36. Toshihide Nakamura, Hiroshi Takagi, and Jun Shima. Effects of ice-seeding temperature and intracellular trehalose contents on survival of frozen Saccharomyces cerevisiae cells. *Cryobiology*, 58(2):170–174, 2009. doi:10.1016/j.cryobiol.2008.11.012.
37. Jun Shima, Akihiro Hino, Chie Yamada-Iyo, Yasuo Suzuki, Ryouichi Nakajima, Hajime Watanabe, Katsumi Mori, and Hiroyuki Takano. Stress Tolerance in Doughs of Saccharomyces cerevisiae Trehalase Mutants Derived from Commercial Baker's Yeast. *Applied and Environmental Microbiology*, 65(7):2841–2846, 7 1999. URL: https://journals.asm.org/doi/10.1128/AEM.65.7.2841-2846.1999, doi:10.1128/AEM.65.7.2841-2846.1999.
38. John H. Crowe, Lois M. Crowe, and Dennis Chapman. Preservation of Membranes in Anhydrobiotic Organisms: The Role of Trehalose. *Science*, 223(4637):701–703, 2 1984. URL: https://www.science.org/doi/10.1126/science.223.4637.701, doi:10.1126/science.223.4637.701.
39. Elis C A Eleutheria, Pedro S. de Araujo, and Anita D. Panek. Role of the trehalose in dehydration resistance of Saccharomyces cerevisiae. *BBA - General Subjects*, 1156(3):263–266, 1993. doi:10.1016/0304-4165(93)90040-F.
40. Ali Eroglu, Michael J Russo, Robert Bieganski, Alex Fowler, Stephen Cheley, Hagan Bayley, and Mehmet Toner. Intracellular trehalose improves the survival of cryopreserved mammalian cells. *Nature Biotechnology*, 18(2):163–167, 2 2000. URL: https://www.nature.com/articles/nbt0200_163http://biotech.nature.com, doi:10.1038/72608.
41. Lei Shi, Benjamin M. Sutter, Xinyue Ye, and Benjamin P. Tu. Trehalose Is a Key Determinant of the Quiescent Metabolic State That Fuels Cell Cycle Progression upon Return to Growth. *Molecular Biology of the Cell*, 21(12):1982–1990, 6 2010. URL: https://www.molbiolcell.org/doi/10.1091/mbc.e10-01-0056, doi:10.1091/mbc.e10-01-0056.
42. Basile Jacquel, Théo Aspert, Damien Laporte, Isabelle Sagot, and Gilles Charvin. Monitoring single-cell dynamics of entry into quiescence during an unperturbed life cycle. *eLife*, 10:1–16, 2021. doi:10.7554/eLife.73186.
43. Linda L. Breeden and Toshio Tsukiyama. Quiescence in Saccharomyces cerevisiae. *Annual Review of Genetics*, 56:253–278, 2022. doi:10.1146/annurev-genet-080320-023632.
44. Viktor M. Boer, Christopher A. Crutchfield, Patrick H. Bradley, David Botstein, and Joshua D. Rabinowitz. Growth-limiting Intracellular Metabolites in Yeast Growing under Diverse Nutrient Limitations. *Molecular Biology of the Cell*, 21(1):198–211, 1 2010. URL: https://www.molbiolcell.org/doi/10.1091/mbc.e09-07-0597, doi:10.1091/mbc.e09-07-0597.
45. Markus Basan, Tomoya Honda, Dimitris Christodoulou, Manuel Hörl, Yu-Fang Fang Chang, Emanuele Leoncini, Avik Mukherjee, Hiroyuki Okano, Brian R. Taylor, Josh M. Silverman, Carlos Sanchez, James R. Williamson, Johan Paulsson, Terence Hwa, and Uwe Sauer. A universal trade-off between growth and lag in fluctuating environments. *Nature*, 584(7821):470–474, 8 2020. URL: http://dx.doi.org/10.1038/s41586-020-2505-4https://www.nature.com/articles/s41586-020-2505-4, doi:10.1038/s41586-020-2505-4.
46. Chris Allen, Sabrina Buttner, Anthony D. Aragon, Jason A. Thomas, Osorio Meirelles, Jason E. Jaetao, Don Benn, Stephanie W. Ruby, Marten Veenhuis, Frank Madeo, and Margaret Werner-Washburne. Isolation of quiescent and nonquiescent cells from yeast stationary-phase cultures. *The Journal of Cell Biology*, 174(1):89–100, 7 2006. URL: http://www.ncbi.nlm.nih.gov/pubmed/16818721http://www.pubmedcentral.nih.gov/articlerender.fcgi?artid=PMC2064167https://rupress.org/jcb/article/174/1/89/53700/Isolation-of-quiescent-and-nonquiescent-cells-from, doi:10.1083/jcb.200604072.
47. Monika Opalek, Bogna Smug, Michael Doebeli, and Dominika Wloch-Salamon. On the Ecological Significance of Phenotypic Heterogeneity in Microbial Populations Undergoing Starvation. *Microbiology Spectrum*, 10(1), 2 2022. URL: https://journals.asm.org/doi/10.1128/spectrum.00450-21, doi:10.1128/spectrum.00450-21.
48. Tomás Alarcón and Henrik Jeldtoft Jensen. Quiescence: A mechanism for escaping the effects of drug on cell populations. *Journal of the Royal Society Interface*, 8(54):99–106, 2011. doi:10.1098/rsif.2010.0130.
49. Anthony D. Aragon, Angelina L. Rodriguez, Osorio Meirelles, Sushmita Roy, George S. Davidson, Phillip H. Tapia, Chris Allen, Ray Joe, Don Benn, and Margaret Werner-Washburne. Characterization of Differentiated Quiescent and Nonquiescent Cells in Yeast Stationary-Phase Cultures. *Molecular Biology of the Cell*, 19(3):1271–1280, 3 2008. URL: https://www.molbiolcell.org/doi/10.1091/mbc.e07-07-0666, doi:10.1091/mbc.e07-07-0666.
50. Felix Keller, Maja Schellenberg, and Andres Wiemken. Localization of trehalase in vacuoles and of trehalose in the cytosol of yeast (Saccharomyces cerevisiae). *Archives of Microbiology*, 131(4):298–301, 6 1982. URL: http://link.springer.com/10.1007/BF00411175, doi:10.1007/BF00411175.
51. Xia Wang, Kotaro Fujimaki, Geoffrey C. Mitchell, Jungeun Sarah Kwon, Kimiko Della Croce, Chris Langsdorf, Hao Helen Zhang, and Guang Yao. Exit from quiescence displays a memory of cell growth and division. *Nature Communications*, 8(1):321, 8 2017. URL: http://dx.doi.org/10.1038/s41467-017-00367-0https://www.nature.com/articles/s41467-017-00367-0http://www.ncbi.nlm.nih.gov/pubmed/28831039http://www.pubmedcentral.nih.gov/articlerender.fcgi?artid=PMC5567331, doi:10.1038/s41467-017-00367-0.
52. Anita Panek. Function of trehalose in Baker's yeast (Saccharomyces cerevisiae). *Archives of Biochemistry and Biophysics*, 100(3):422–425, 3 1963. URL: https://linkinghub.elsevier.com/retrieve/pii/0003986163901073, doi:10.1016/0003-9861(63)90107-3.
53. Claudio de Virgilio. The essence of yeast quiescence. *FEMS Microbiology Reviews*, 36(2):306–339, 2012. doi:10.1111/j.1574-6976.2011.00287.x.
54. T Chen, J P Acker, a Eroglu, S Cheley, H Bayley, a Fowler, and M Toner. Beneficial effect of intracellular trehalose on the membrane integrity of dried mammalian cells. *Cryobiology*, 43(2):168–81, 2001. URL: http://www.ncbi.nlm.nih.gov/pubmed/11846471, doi:10.1006/cryo.2001.2360.
55. Peter Mazur. Physical and Temporal Factors Involved in the Death of Yeast at Subzero Temperatures. *Biophysical Journal*, 1(3):247–264, 1 1961. URL: https://linkinghub.elsevier.com/retrieve/pii/S0006349561868872, doi:10.1016/S0006-3495(61)86887-2.
56. J. B. Griffiths, C. S. Cox, D. J. Beadle, C. J. Hunt, and D. S. Reid. Changes in cell size during the cooling, warming and post-thawing periods of the freeze-thaw cycle. *Cryobiology*, 16(2):141–151, 1979. doi:10.1016/0011-2240(79)90024-5.
57. Tani Chen, Alex Fowler, and Mehmet Toner. Literature review: Supplemented phase diagram of the trehalose-water binary mixture. *Cryobiology*, 40(3):277–282, 5 2000. URL: https://linkinghub.elsevier.com/retrieve/pii/S0011224000922442, doi:10.1006/cryo.2000.2244.
58. Siraje Arif Mahmud, Takashi Hirasawa, and Hiroshi Shimizu. Differential importance of trehalose accumulation in Saccharomyces cerevisiae in response to various environmental stresses. *Journal of Bioscience and Bioengineering*, 109(3):262–

266, 2010. URL: http://dx.doi.org/10.1016/j.jbiosc.2009.08.500, doi:10.1016/j.jbiosc.2009.08.500.

59. Z CAKAR, U SEKER, C TAMERLER, M SONDEREGGER, and U SAUER. Evolutionary engineering of multiple-stress resistant. *FEMS Yeast Research*, 5(6-7):569–578, 4 2005. URL: https://academic.oup.com/femsyr/article-lookup/doi/10.1016/j.femsyr.2004.10.010, doi:10.1016/j.femsyr.2004.10.010.
60. Monika Opalek, Hanna Tutaj, Adrian Pirog, Bogna J. Smug, Joanna Rutkowska, and Dominika Wloch-Salamon. A Systematic Review on Quiescent State Research Approaches in S. cerevisiae. *Cells*, 12(12):1608, 6 2023. URL: https://www.mdpi.com/2073-4409/12/12/1608, doi:10.3390/cells12121608.
61. Dominika M. Wloch-Salamon, Katarzyna Tomala, Dimitra Aggeli, and Barbara Dunn. Adaptive Roles of SSY1 and SIR3 During Cycles of Growth and Starvation in Saccharomyces cerevisiae Populations Enriched for Quiescent or Nonquiescent Cells. *G3 Genes|Genomes|Genetics*, 7(6):1899–1911, 6 2017. URL: https://academic.oup.com/g3journal/article/7/6/1899/6029837, doi:10.1534/g3.117.041749.

Supplementary Information

Materials and Methods

Strains and growth

The yeast strain *Saccharomyces cerevisiae* CEN.PK a/α obtained from Laxman lab (InStem) was used as wild type to evolve increased tolerance to freeze thaw. Cultures were grown in rich nutrient media called YPD (Yeast extract [1%] (HIMEDIA, Catalog no. - RM027), Peptone [2%] (HIMEDIA, Catalog no. - RM014), Dextrose [2%] (Qualigens, Catalog no. - Q15405), with 2% agar (HIMEDIA, Catalog no. - GRM026) for plates).

Freeze-thaw

500 μl of stationary phase culture was aliquoted into 1.5 ml microcentrifuge tubes. Freezing was done by immersing the tubes in liquid nitrogen for 15 minutes, unless stated otherwise. The culture was then thawed by removing the tubes from liquid nitrogen and immersing them in room temperature water for 15 minutes.

Selection to freeze thaw

Figure 1 shows the protocol followed to select for adaptation to freeze-thaw stress. Yeast cultures were grown for 24 hours ($\approx$12 generations) to attain stationary phase. The culture was then put through either one freeze-thaw or three freeze-thaws according to the experiment. The cells that survived the freeze-thaw(s) were grown in fresh media and the cycle of freeze-thaw(s)-growth was repeated until the survival levels saturated. For the controls, the same protocol was followed without the freeze-thaw procedure.

Survival measurements

Survival in cells/ml was measured for each cycle during the evolution by checking for Colony Forming Units (CFUs) on a YPD agar plate. The concentration of viable cells was measured before and after the freeze-thaw(s) to estimate the fraction of cells that survived the freeze-thaw(s). Cell culture was appropriately diluted and added to a Petri dish with YPD agar poured into it along with 4-7 glass beads. The culture was then spread on the plate by shaking the petri dish and the beads were discarded. The petri dishes were then incubated in a 30° C incubator for 48 hours. The petri dishes were then imaged and the number of cell colonies formed were counted.

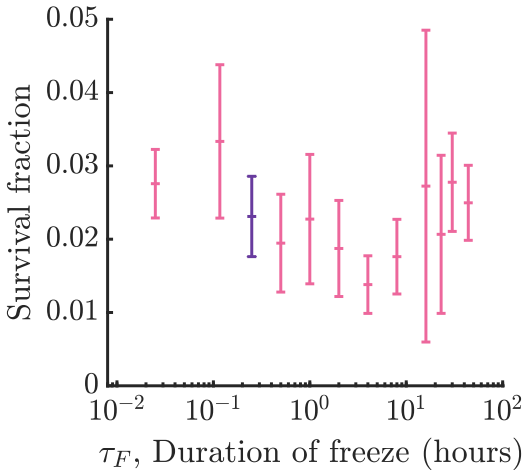

Figure S1. Survival fraction of cells measured over different freeze durations

Membrane damage and survival measurements

Lysis of cells after freeze-thaw was checked using BD FACSVerse™ Cell Analyzer by measuring the concentration of intact cells before and after freeze-thaw. To investigate membrane damage, cells were stained using the Funga-Light™ Yeast CFDA, AM/Propidium Iodide Vitality Kit (Invitrogen, Catalog no. - F34953). Cells were then analysed using a BD FACSAria™ Fusion Flow Cytometer. The cells clustered into two populations on the CFDA vs propidium iodide plot - one membrane-damaged population and one membrane intact population. The two populations were sorted and the concentration of cells in each population was analysed on the BD FACSVerse™ Cell Analyzer. Further, the sorted cell cultures were treated with 50 ug/ml Ampicillin and spread on YPD agar plates with appropriate dilutions to measure survival by counting the number of Colony Forming Units (CFUs). A membrane damage metric

was obtained from the fluorescence intensities of propidium iodide (PI) and 5-CFDA (CFDA) combined as follows:

$$\text{Membrane damage} = \frac{\frac{\log(\text{PI})}{\log(\max(\text{PI}))} + 1 - \frac{\log(\text{CFDA})}{\log(\max(\text{CFDA}))}}{2} \quad \textbf{(S1)}$$

Cell morphology measurements

Cells were imaged at stationary phase to measure their size and shape. Brightfield imaging on cells was performed using an inverted Olympus IX-81 microscope equipped with a Photometrics Prime sCMOS camera, a motorized stage, 100x/1.4NA UPlanSApo oil immersion objective and controlled with OLYMPUS cellSens Dimension software. The area and eccentricity of cells was then measured from these images using custom written MATLAB code. The fraction of cells budding was manually counted from these images.

Single cell mass density measurements

Single cell mass density was measured using a Percoll gradient column. Stock Isotonic Percoll (SIP) was made by adding 1.5M sodium chloride to Percoll™ (GE Healthcare life sciences, Catalog no. - 17-0891-01) in a 1:9 ratio. SIP was diluted with 0.15M sodium chloride to make 70%, 80% and 90% density solutions. 1.5 ml of each of these solutions was aliquoted in different 2 ml microcentrifuge tubes. The tubes were centrifuged at 20,000g at 4° C for 15 minutes to prepare density gradient columns. 500 μl of stationary phase cells were washed once in Phosphate Buffered Saline (PBS) by centrifugation at 200g for 2 minutes and resuspended in 100 μl PBS. Density was calibrated by using a mixture of Density Marker Beads (Cospheric, DMB-kit). After the density gradient columns were prepared, 100 μl of cell and bead suspensions were gently added at the top of the columns ad centrifuged for 1 hour at 400g at room temperature. The columns were then imaged using a phone's camera and the position of cells was measured to calculate their density.

Population biomass measurements

Dry mass of cells of the population was measured at stationary phase. PVDF syringe filters (Millipore, Catalog no. - SLGVR33RS) 33mm wide with a pore size of 0.22um were initially weighed. The filter was attached to a syringe and 10 ml of cell culture was passed through the filter by attaching a vacuum aspirator to the other end of the filter. The filter was alternately kept in a desiccator and a 70° C oven for 5 minutes each three times. The filter was then left in the 70° C oven overnight and subsequently weighed to measure the residual dry cell mass.

DNA fluorescence intensity measurements

Cells were stained with SYTOX Green based on a previous protocol (1). 3ml of stationary phase culture was centrifuged at 1500g for 2 minutes at room temperature to remove media. The cells were fixed in 70% ethanol and incubated for 16 hours at 4° C. Cells were then pelleted and washed in 50mM sodium citrate buffer (pH 7.5). The cell pellet was re-suspended in 500 μl RNAse A buffer (500ul sodium citrate buffer + 5ul RNAse A) and incubated at 50° C for 2 hours with shaking. Cells were then washed and resuspended in 50mM sodium citrate and incubated at 30° C for 3 hours with shaking. Cells were pelleted and resuspended in Proteinase K solution (20ul enzyme (2mg/ml) + 180ul sodium citrate buffer). They were incubated for 37° C for 1 hour, with shaking. Following Proteinase K treatment, cells were pelleted, washed and resuspended in 1 ml of sodium citrate buffer and incubated overnight at 30° C with shaking. The sample was diluted 20 times and 1 drop of SYTOX Green was added to 500ul of the sample. The samples were then analysed using flow cytometry. The SYTOX green fluorescence intensity was acquired through the FITC channel.

Measurement of cell relaxation during cell wall digestion

Brightfield imaging of cell relaxation was done on an Olympus IX-81 microscope in a polydimethylsiloxane (PDMS) chamber. The PDMS chamber was made by pouring PDMS mixed with a curing agent in a 10:1 ratio in a silicon wafer mould of a well 1cm x 2cm with a height of 50um. PDMS was heat cured and covalently bonded to a coverglass by plasma cleaning after making two holes for injecting cells. The device was pre-soaked in water overnight and used 15 minutes after being removed from the water. 1ml of stationary phase cell culture was washed twice in Sorbitol buffer (1.2M D-Sorbitol in Phosphate Buffered Saline) by centrifuging at 1500g for 1.5 minutes. Cells were incubated in 0.2% 2-mercaptoethanol in Sorbitol buffer at 30° C for 45 minutes with shaking. The cells were then washed three times with enzyme buffer (Sorbitol buffer + glucose 1%) by centrifuging at 1000g for 2 minutes. Cells were concentrated to double the concentration and 0.25mg/ml Zymolyase was added. The cell reaction suspension was injected into the PDMS chamber. The chamber was sealed with vacuum grease to prevent evaporation. The chamber was placed in a stage-top incubator with a water bath to maintain temperature at 30° C with humidity. Cells were imaged using a 60x objective with an interval of 1 minute during the course of cell wall relaxation and images were analyzed to measure the eccentricity of cells over time.

Deformability cytometry

Deformability cytometry was performed on cells with a protocol based on a previous study by Otto *et al.* (2).

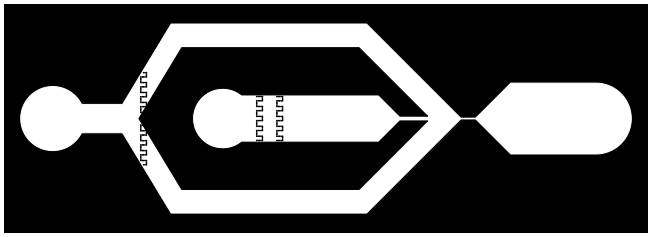

Figure S2. Design of the deformability cytometry device

Microfluidic Device Preparation The microfluidic device was made using polydimethylsiloxane (PDMS) (Sylgard 184; Dow Corning) from a silicon wafer mould and bonded to a coverglass. The silicon wafer mould was fabricated using a soft lithography protocol in a clean room from a quartz mask with design as shown in S2. The following steps detail the protocol for fabrication of the silicon wafer mould:

1. A silicon wafer was washed with acetone, ethanol and isopropyl alcohol and air dried.
2. It was then placed on a hot plate at 95° C for 20 minutes for all the solvent to evaporate.
3. The wafer was plasma cleaned for 10 minutes.
4. The wafer was spin coated with SU 8 5 with the following parameters:

Cycle	Hold (Time (s))	Speed (rpm)	Acceleration
1	5	500	200
2	30	875	300

Table 1. Parameters for spin coating

5. The wafer was pre-softbaked at 65° C for 3 minutes.
6. It was then softbaked at 95° C for 12 minutes.
7. The quartz mask was placed on the silicon wafer in a mask aligner and exposed to UV light for 3 seconds using vacuum contact.
8. Pre post exposure bake was done at 65° C for 1 minute.
9. Post exposure bake was done at 95° C for 4 minutes.
10. The silicon wafer was washed with developer for 3 minutes.
11. It was then washed with isopropyl alcohol and acetone
12. The wafer was finally dried on a hot plate at 95 ° C.
13. The features were measured on a profilometer.

The following steps elaborate the protocol used for preparation of PDMS devices from the silicon wafer:

1. PDMS and the cross linker were mixed thoroughly in a 10:1 ratio and poured over the silicon wafer mould.
2. The PDMS was placed in a desiccator for degassing until it was completely free of bubbles.
3. PDMS was cured at 70° C for two hours.
4. The device was cut out and holes were punched for inserting tubing at the inlet and outlet.
5. The PDMS was cleaned with scotch tape. A coverglass was cleaned with Hellmanex, ethanol and isopropyl alcohol and air dried.
6. The PDMS and coverglass were plasma cleaned for 3 minutes.
7. The PDMS was covalently bonded to the coverglass by placing the two in contact with each other and pressing lightly.
8. The microfluidic device was then placed at 70° C for 10 minutes to ensure complete bonding.

Solutions:

- 0.5% 2-hydroxyethyl cellulose (Sigma Aldrich, Catalog no. - 434981) + 1.2M Sorbitol in PBS (buffer for cells and sheath fluid)
- 1.2M Sorbitol in PBS (SB, for spheroplasting)
- 1.2M Sorbitol + 1% Glucose in PBS (SB+Glc, for spheroplasting)
- 100% 2-mercaptoethanol (BME, for spheroplasting)

Material:

- Two 250uL Glass Syringes (Hamilton, 1725)
- Syringe Pump (Harvard Apparatus, Pump33 DDS)
- Two Needles (Dispovan 1.2 x 38 mm)
- Three pieces of silicon tubing (OD 1.65 mm, Dow Corning Silastic)
- Deformability cytometry microfluidic device

Viscous Buffer Preparation Procedure The following ingredients were used for preparation of the viscous buffer used to shear cells :

- 100 mL Autoclaved Phosphate Buffered Saline (Sigma Aldrich, Catalog no. - P3813)
- 0.5g 2-Hydroxyethyl cellulose, with a molecular weight around 1.3×10^6 (Sigma Aldrich, Catalog no. - 434981)
- 21.8604g D-Sorbitol (Sigma Aldrich, Catalog no. - S1876)

Procedure:

1. 0.5g of 2-Hydroxyethyl Cellulose was added to 100 mL of autoclaved PBS.
2. The mixture was stirred at 65℃ until the cellulose dispersed homogeneously. This process, lasting about 2 hours, resulted in increased viscosity and a slight turbidity.
3. 21.8604g of Sorbitol was added to obtain a concentration of 1.2M. Stirring at room temperature continued for a few hours until the solution turned clear.
4. The solution was filtered using a 0.22μm Merck syringe filter and left at room temperature.

Cell Spheroplasting

- 1 ml of stationary phase cell culture was centrifuged at 1500g for 1.5 minutes.
- The cell pellet underwent two washes with Sorbitol in PBS (SB) by centrifuging at 1500rcf for 1.5 minutes.
- The washed cells were resuspended in 1 mL of SB with the addition of 2 µL of 100% 2-mercaptoethanol (BME).
- The cells were then incubated at 30 ° C for 45 minutes.
- After BME treatment, cells underwent further washing (3 times with Sorbitol + 1% Glucose in PBS (SB+Glc)) by centrifuging at 1000rcf for 2 minutes.
- A mixture of 1 mL SB+Glc and 100 µL of 2.5 mg/mL Zymolyase was added to the cells, and the suspension was incubated at 30℃.
- The WT cells were incubated for 1 hour, while the EVO cells were incubated for 4 hours.
- The resulting spheroplasts were washed twice with SB by centrifuging at 1000rcf for 2 minutes.
- Spheroplasts were resuspended in the prepared buffer.
- The suspension was subjected to vortexing for 2 minutes to break up the clumps.
- A bumpy surface, such as a pipette tip rack, was employed for additional clump disruption.
- The suspension was degassed in a desiccator for 1 minute to eliminate air bubbles.

Microfluidic Device Setup:

- Two clean and dry glass syringes were wiped with 70% ethanol.
- Silicon tubing was connected to the syringes using needles.
- The tubing was cleaned with an air gun and the free ends of the tubing were wiped with 70% ethanol.
- The sheath syringe and its tubing were filled with filtered buffer, ensuring that the tubing was submerged in buffer to avoid air bubbles.
- The cell syringe and its tubing were filled with spheroplasts in buffer, avoiding air bubbles.
- Sheath tubing, followed by cell tubing and discard tubing, were carefully inserted into the designated holes of the microfluidic device, using coverage of other holes with Scotch tape to prevent debris ingress.

Imaging and Flow setup

- Images were acquired on an Olympus IX-81 inverted microscope with a Phantom Miro X4 high-speed camera using a 60X oil objective. The camera was controlled using Phantom Camera Control (PCC) 3.4 software.
- Syringes were connected to the syringe pump and the free end of the discard tube was placed in a microcentrifuge tube secured to the stage.
- The inlets were filled with sheath fluid and cells. The rest of the device was then filled with sheath fluid.
- Then, the sheath fluid was set to flow at the specified rate followed by cells.
- The camera was focused to capture cells as they exited the channel, ensuring a consistent region of interest (ROI).
- The following camera parameters were used:
  - Resolution = 128 x 64
  - FPS = 40k
  - Exposure = 4us
  - Brightness = 0
  - Gain = 0.73
  - Gamma = 0.95
  - Sensitivity = 2.5
- The system was monitored until the flow stabilized, as indicated by a constant number of frames for a cell to travel a fixed distance.
- A waiting time of 10-15 minutes was necessary for flow stabilization.
- Movies were stored as .cine files for fast acquisition.

Analysis The .cine files were first converted to smaller files in TIFF format using the PCC software such that the first frame was empty to use as background image for segmentation. Image segmentation and data analysis were performed using custom written code on MATLAB.

Kinetics of cell disintegration

Cell culture in stationary phase was centrifuged at 1500g for two minutes and the supernatant was removed. Half the initial volume of Sorbitol Buffer was added and cells were treated with 0.2% 2-mercaptoethanol for 45 minutes at 30° C with shaking. Cells were then washed three times with Enzyme Buffer by centrifuging at 1500g for two minutes. 0.25mg/ml Zymolyase was added to cells in the Enzyme Buffer and this reaction mixture was tested for spheroplasting. Cells in Enzyme Buffer was used as the control. 200ul of the reaction mixtures and controls were aliquoted into one set of wells of a 96-well plate. The plate was incubated at 30° C with shaking in a Spark® multimode plate reader throughout the experiment. At each time point, the plate was moved out, 30ul of reaction mixture (or control) and 150ul of water was added to a well and the absorbance was measured at 800nm.

Cloning of GEMs gene into HO-poly-kanMX4-HO Plasmid Vector

Bases 3119 to 5315 of the *pRS305-Leu2-PINO4-Pfv-GS-Sapphire* plasmid (AddGene, Plasmid # 116930) were inserted into the *HO-poly-kanMX4-HO* plasmid vector (AddGene, Plasmid # 51662, obtained from Laxman lab, InStem). The region of the *HO-poly-KanMX4-HO* plasmid vector for cloning was determined based on the restriction enzyme sites BsaBI and BsiWI.

Primer Design and PCR Optimization Primers were designed for PCR amplification of the yeGFP region and their parameters were tested using oligoanalyzer. The annealing temperature for the PCR was determined to be 62℃ for template copying, with a first step annealing temperature of 55℃. Gradient PCR was performed to find the optimal annealing temperature.

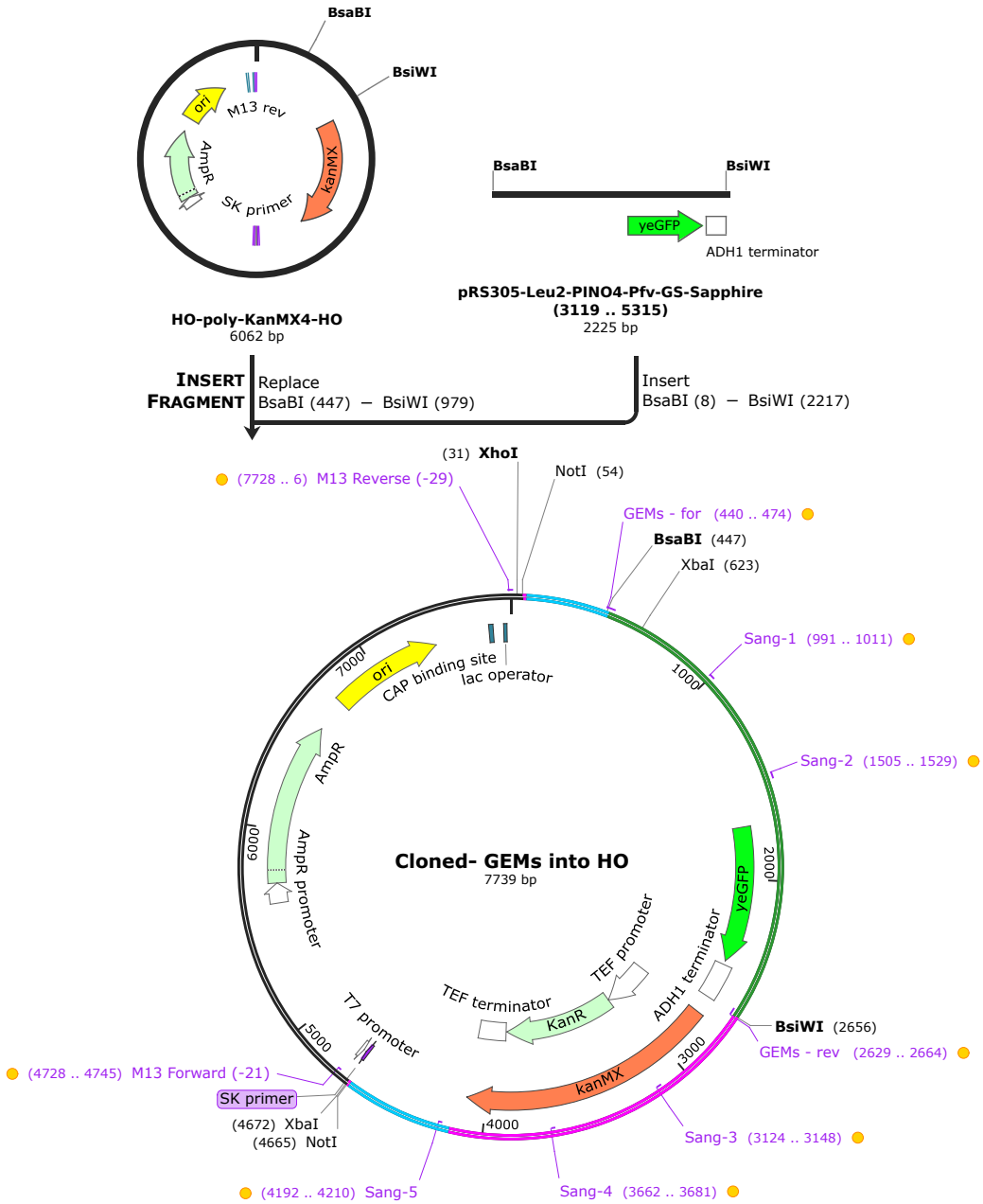

Figure S3. Map of cloned GEMs Plasmid

Plasmid Isolation Bacterial cultures containing the *HO-poly-KanMX4-HO* plasmid vector (obtained from Laxman lab, InStem) and the *pRS305-Leu2-PINO4-Pfv-GS-Sapphire* plasmid were inoculated into Luria Broth + Ampicillin (100 µg/ml) and incubated at 37℃. Plasmid isolation was performed using a MiniPrep kit (QIAGEN, Catalog no. - 27104). Plasmid quality and concentrations were measured using a TECAN NanoQuant plate reader.

PCR Amplification The PCR amplification of the yeGFP region from the *pRS305-Leu2-PINO4-Pfv-GS-Sapphire* plasmid was performed using KOD hotstart DNA polymerase kit with the following components in the reaction mixture:

Component	**Final concentration**	**Volume**
10X buffer	1X	5 μl
25mM MgSO4	1.5 mM	3 μl
DNTPs (2 nM each)	0.2 mM(each)	5 μl
Sense primer (10 μM)	0.3 μM	1.5 μl
Anti-sense primer (10 μM)	0.3 μM	1.5 μl
Plasmid	1ng/μl	1 μl
Water		32 μl
Polymerase (1 U/μl)	0.02U/μl	1 μl
Total		50 μl

Based on the 2200bp length of the fragment, the following parameters were used for the PCR:

1. Polymerase activation : 95° C for 2 minutes
2. Denaturation : 95°C for 20s
3. Annealing : 54.3°C for 30s
4. Extension : 70°C for 45s
5. Repeated steps 2-4 for 35 cycles
6. Annealing remaining : 54.3°C for 5 mins
7. Temperature was set to 4°C.

PCR Purification and Product Analysis The PCR products were purified using a PCR purification kit (QIAGEN, Catalog no. - 28104) to remove other reactants. Purified plasmid quality and concentrations were measured using a TECAN NanoQuant plate reader.

Restriction Enzyme Digestion The purified PCR products and the *HO-poly-KanMX4-HO* plasmid vector were separately digested using BsiWI-HF and BsaBI-HF restriction enzymes. using the following protocol:

1. The following reaction mixtures were prepared:

   PCR product (purified)

Nuclease free water	84 μl
PCR product	4 μl
CutSmart	10 μl
BsiWI-HF	2 μl
total	100 μl

   HO-poly-KanMX4-HO plasmid

2. The reaction mixtures were incubated at 37°C for 4:10 hours.
3. 2ul of BsaBI was added and the reaction mixtures were incubated at 60°C for 3 hours.
4. The digested products were purified using a PCR purification kit (QIAGEN, Catalog no. - 28104) to remove restriction enzymes and other reactants.

Nuclease free water	82 μl
Plasmid	6 μl
CutSmart	10 μl
BsiWI-HF	2 μl
total	100 μl

Water	41 μl
pCK01 (1000ng/μl)	5 μl
CutSmart	3 μl
NotI-HF	1 μl
Total	50 μl

5. The purified digested products were analysed using a TECAN NanoQuant plate reader.
6. The digested *HO-poly-KanMX4-HO* plasmid was run on a 1% agarose gel prepared with 50ml TAE and 2ul SYBR green dye at 100V for 3 hours alongwith an appropriate ladder.
7. The required 5.5kb band was cut out under UV.
8. The gel band was purified using a gel purification kit (QIAGEN, Catalog no. - 28704).
9. The purified product was analyzed on an agarose gel to confirm the presence of the desired DNA fragments.

Ligation The insert was ligated into the vector using T4 DNA ligase (NEB). Different ratios of vector to insert were tested for ligation efficiency. The ligation mixtures were incubated at 16°C overnight. The ligation mixtures were then heat inactivated by incubating at 65°C for 10 minutes.

Transformation into Bacteria The ligation mixtures were transformed into competent *DH5*α cells using the following protocol:

1. Competent cells at -80°C were thawed on ice.
2. 20 μl of ligation mixture was added to the competent cells and incubated on ice for 30 minutes.
3. A heat shock was provided by heating 42°C for 90s and then keeping on ice for 90s.
4. 50ul of the cell suspension was added to 1 ml of LB.
5. Cells were incubated at 37°C for 1 hour with shaking.
6. The transformed cells were plated onto LB+Kanamycin agar plates and incubated overnight at 37°C.

Colonies from the transformed plates were picked and subjected to colony PCR using Taq pol and gel electrophoresis to confirm successful transformation.

Plasmid Isolation and Sequencing Plasmids from positive colony PCR samples were isolated using the MiniPrep kit and submitted for Sanger sequencing to verify the sequence with primers as shown in S3.

Restriction Enzyme Digestion for Transformation The plasmid was digested with NotI prior to transformation in order to be integrated into the yeast genome using the following protocol: The reaction mixture was incubated at 37°C for 6 hours followed by 4°C to stop the reaction.

Yeast Transformation

1. 10ml yeast cell culture was grown to 1 OD.
2. A 1.0 ml sample of carrier DNA at a concentration of 2 mg/ml (salmon sperm) was boiled for 5 minutes and chilled in an ice/water bath. 1 mg/ml of carrier DNA was used in the reaction.
3. Yeast cells were spun down at 3000g for 1 minute.
4. The pellet was resuspended in approximately 1 ml of water and spun down again in a 1.5 ml microcentrifuge tube at 1000g for 1 minute.
5. The pellet was washed by resuspending in 800 μl of 0.1 M Lithium Acetate (LiAc) and spinning down the cells at 1000g for 1 minute.
6. The following reagents were added to prepare the transformation mix:
   - PEG 3500 (50% w/v, sterile filtered): 240 μl
   - Lithium Acetate (1.0 M): 35 μl

- Boiled (salmon sperm) carrier DNA: 25 μl
- 2 µg NotI digested plasmid + water: 50 μl

7. 350 μl of the transformation mix was added to the cells and vortexed vigorously.
8. Incubation was carried out at 30°C for 30 minutes.
9. The tubes were then incubated in a 42°C water bath for 30 minutes.
10. Centrifugation was performed at 1000g for 1 minute, and the transformation mix was removed.
11. 1.0 ml of YPD was pipetted into each tube; the pellet was stirred with a micropipette tip and vortexed.
12. Cells were spun down in the culture tube, media was removed, and they were resuspended in 100 μl water. This 100 μl was plated onto YPD agar plates + G418.
13. The plates were incubated at 30°C until colonies appeared.

Colony Selection and Culturing Transformed yeast colonies were selected, inoculated into YPD medium, and cultured overnight. A -80°C stock of the culture was prepared for long-term storage.

Particle tracking of GEMs

Single particle tracking of the GEM particles was performed on cells spread on an agar pad. The particles were imaged on a Nikon eclipse Ti microscope in partial TIRF mode using a 100x 1.45 NA Plan TIRF objective and a 488 excitation. Images were acquired every 5ms on a Photometrics prime 95B sCMOS camera. Particles were tracked and trajectories were analysed using custom written MATLAB code.

Mean squared displacement analysis

The time-averaged mean squared displacement (MSD) for a single particle i in terms of its x and y coordinates is calculated as:

$$\langle \Delta r^2(t) \rangle_{\text{time},i} = \frac{1}{T-t} \sum_{\tau=0}^{T-t} \left[(x_i(\tau+t) - x_i(\tau))^2 + (y_i(\tau+t) - y_i(\tau))^2 \right], \quad \textbf{(S2)}$$

where:

- $x_i(\tau)$ and $y_i(\tau)$ are the x- and y-coordinates of particle i at time τ,
- t is the lag time,
- T is the total observation time for the trajectory of each particle.

This equation calculates the MSD for a single particle by averaging its squared displacements over all possible starting points τ for a given lag time t. The time and ensemble-averaged MSD, which considers all N particles, is given by:

$$\langle \Delta r^2(t) \rangle = \frac{1}{N} \sum_{i=1}^{N} \langle \Delta r^2(t) \rangle_{\text{time},i}, \quad \textbf{(S3)}$$

or equivalently:

$$\langle \Delta r^2(t) \rangle = \frac{1}{N} \sum_{i=1}^{N} \frac{1}{T-t} \sum_{\tau=0}^{T-t} \left[(x_i(\tau+t) - x_i(\tau))^2 + (y_i(\tau+t) - y_i(\tau))^2 \right], \quad \textbf{(S4)}$$

where N is the total number of particles. The exponent, α, was obtained by fitting the obtained time-averaged MSD to a power law for $t = 0.005$ s to $t = 0.05$ s for a given particle.

Whole genome sequencing

For each evolution experiment, the starter culture, evolved strains, and control strains were sequenced. The evolved and control samples were collected from the middle and end of the evolution experiment. 13 samples were sequenced for each evolution experiment. Samples aliquoted and stored at -80°C during the evolution experiment were inoculated and grown as a liquid culture to stationary phase. DNA from cells of these cultures was isolated using a Phenol:Chloroform:Isoamylalcohol extraction method. A DNA library was generated from this using the library preparation kit - Illumina® DNA Prep, (M) Tagmentation (Catalog no. - 20018705). The library was then amplified by PCR and sequenced on the NovaSeq 6000 platform using an SP flowcell with a sequencing read length of 2x100bp to obtain paired-end reads for all 26 samples.

Sample	Description
CTPO	Parent strain for one freeze-thaw tolerance selection
CTPT	Parent strain for three freeze-thaw tolerance selection
CTC1M1	Control sample 1 of one freeze-thaw selection at mid-point of evolution
CTC1M2	Control sample 2 of one freeze-thaw selection at mid-point of evolution
CTC3M1	Control sample 1 of three freeze-thaw selection at mid-point of evolution
CTC3M2	Control sample 2 of three freeze-thaw selection at mid-point of evolution
CTF1M1	Replicate 1 of one freeze-thaw selection at mid-point of evolution
CTF1M2	Replicate 2 of one freeze-thaw selection at mid-point of evolution
CTF1M3	Replicate 3 of one freeze-thaw selection at mid-point of evolution
CTF1M4	Replicate 4 of one freeze-thaw selection at mid-point of evolution
CTF3M1	Replicate 1 of three freeze-thaw selection at mid-point of evolution
CTF3M2	Replicate 2 of three freeze-thaw selection at mid-point of evolution
CTF3M3	Replicate 3 of three freeze-thaw selection at mid-point of evolution
CTF3M4	Replicate 4 of three freeze-thaw selection at mid-point of evolution
CTC1E1	Control sample 1 of one freeze-thaw selection at end-point of evolution
CTC1E2	Control sample 2 of one freeze-thaw selection at end-point of evolution
CTC3E1	Control sample 1 of three freeze-thaw selection at end-point of evolution
CTC3E2	Control sample 2 of three freeze-thaw selection at end-point of evolution
CTF1E1	Replicate 1 of one freeze-thaw selection at end-point of evolution
CTF1E2	Replicate 2 of one freeze-thaw selection at end-point of evolution
CTF1E3	Replicate 3 of one freeze-thaw selection at end-point of evolution
CTF1E4	Replicate 4 of one freeze-thaw selection at end-point of evolution
CTF3E1	Replicate 1 of three freeze-thaw selection at end-point of evolution
CTF3E2	Replicate 2 of three freeze-thaw selection at end-point of evolution
CTF3E3	Replicate 3 of three freeze-thaw selection at end-point of evolution
CTF3E4	Replicate 4 of three freeze-thaw selection at end-point of evolution

Table 2. Sequenced samples

Sequencing analysis

Quality checks on sequencing output The initial quality of sequencing reads was checked using FastQC. Three of the 11 tests—sequence content, GC content, and duplication level—returned quality failure or warning for all 52 sample files.

Preparation of reads for mapping Trimmomatic was used to filter and trim reads prior to mapping. Bases were trimmed from either end if their quality was below 20. Additionally, the first 20 bases were removed regardless of their quality. Illuminaclip command was used to remove adapter sequence contaminants from read sequences. Trimmomatic first searches for a near exact match of a short adapter segment, of a maximum of 16 bp, within reads and then attempts to extend such "seed" sequences. A maximum of two mismatches were permitted in the seed sequences. A score of 30 ($\sim$50 bases match) was required to consider the read a palindromic match (when the read-through was detectable on both reads of a pair) and a score of 10 for a direct match. The minimum adapter length required to be detected was set to 2 in the palindromic mode. Both reads were retained after the clipping. Reads of a minimum length of 60 after clipping were retained. The adapter sequence used was “CTGTCTCTTATACACATCT”, specific to the sequencing platform. The following command was run to apply the above-mentioned filters:

```
TrimmomaticPE -threads <NCPU> -phred33 -trimlog <log-file> <read-1> <read-2> -baseout
↪  <read-out> ILLUMINACLIP:<adapter-file>:2:30:10:2:True LEADING:20 TRAILING:20 HEADCROP:20
↪  MINLEN:60
```

Mapping of reads to reference The diploid strain CEN.PK113-7D a/α, Assembly accession: GCA_002571405.2_-ASM257140v2 (3) was used as the reference genome to map the filtered and trimmed reads. The BWA-MEM algorithm was used to align paired-end reads to the reference genome with default parameters. Option `-M` was used to mark short split hits as secondary alignments that were to be ignored by downstream tools. Summary statistics for alignment and depth of coverage for every reference position were collected using samtools; flagstat and depth, respectively.

```
bwa mem -M -t <NCPU> -R "@RG\tID:ScerFTE\tSM:<SAMPLE>\tPL:ILLUMINA" <REF> <read-1> <read-2>
↪  | samtools sort -@ <NCPU> -o <sorted.bam> -
```

```
samtools flagstat --threads <NCPU> <sorted.bam> > <summary.flagstat>
```

```
samtools depth <sorted.bam> > <cov.txt>
```

Variant calling SNPs and Indel variants were called for all samples together using `bcftools mpileup` with both minimum base quality and mapping quality set to 20, with option `-per-sample-mF` (minimum number and fraction of gapped reads) to increase the sensitivity of indel detection. Additionally, the `-redo-BAQ` option was used since BAQ (Base Alignment Qualities) has been proposed as a solution to find SNPs around indels, as an alternative to realignment around indels (4). Base qualities (BQ) for variant calls were replaced with min{BQ, BAQ}. A maximum of 1000 reads per input alignment file was used for a position. The multi-allelic caller was used, with a ploidy of 2.

```
bcftools mpileup --redo-BAQ --min-BQ 20 --min-MQ 20 --per-sample-mF --annotate
↪  "FORMAT/AD,FORMAT/ADF,FORMAT/ADR,FORMAT/DP,FORMAT/SP,INFO/AD,INFO/ADF,INFO/ADR"
↪  --threads <NCPU> -d 1000 -f <REF> -b <sorted.bam> -Ou | bcftools call -mv --threads
↪  <NCPU> --ploidy 2 -Ob -o <variants.bcf>
```

Variant filtering All filtering operations were performed using bcftools. First, the SNP and Indel variants were separated. Appropriate thresholds for various variant quality statistics were derived by treating the variants shared by both parental samples as true variants and the variants private to either parent as false variants. This was done in the following steps:
Variants of either type present in parental samples were extracted using the following command:

```
bcftools view -s <sample1,sample2> -a --min-ac 1
```

Option `-a` was used to remove alternative alleles from ALT not seen in the subset. Option `-min-ac` was used to only print the line with at least 1 non-reference allele remaining. The following command listed variants present in only 1 sample *i.e.*, private variants:

```
bcftools view -s <sample1> -x -v <snps/indels>
```

Option `-x` was used to print sites where only the subset of samples have a non-ref allele. Option `-v` was used to extract SNP or Indel variant types.
Further, the private variant files for the parental samples CKC1P1 and CKC3P1 were merged. This list was subtracted from the collection of all parental variants to get a list of variants shared by both parents. Variants that were mutant homozygous in both samples were extracted and used as true variants (182 SNPs + 186 Indels). Heterozygous variants were extracted from the set of private variants and used as false variants (143 SNPs + 142 Indels).

```
bcftools merge <sample1.vcf.gz> <sample2.vcf.gz>
```

```
bcftools isec -p <shared> -c all -C <parental.vcf.gz> <private.vcf.gz>
```

```
bcftools view -i 'COUNT(GT="AA")=2' <shared>/0000.vcf
```

```
bcftools view -i 'COUNT(GT="RA")=1' <private.vcf>
```

The following thresholds were used based on variant quality statistics: SNPs:

- `QUAL >= 50` (Variant Quality)
- `DP <= 20000` (Depth)
- `MQB > 1E-20` (Mapping Quality Bias)
- `BQB > 1E-20` (Base Quality Bias)
- `RPB > 1E-20` (Read Position Bias)
- `SP <= 50` (Strand Bias)

Indels:

- `QUAL >= 50` (Variant Quality)
- `IDV >= 20` (Number of Supporting Reads)

- `IMF >= 0.1` (Fraction of Supporting Reads)

The variants were filtered based on these thresholds using the following commands:

```
bcftools filter -i 'QUAL>=50 && INFO/DP<=20000 && RPB>1e-20 && MQB>1e-20 && BQB>1e-20'
↪  <snps_raw_all.vcf> | bcftools filter -e 'FMT/SP>50'
bcftools filter -i 'QUAL>=50 && IDV>=20 && IMF>=0.1' <indels_raw_all.vcf>
```

Variants passing the above filters were then separated by experiments, and samples were rearranged based on time. Indels separated by only 3 or fewer bases were filtered out (filter -G 3).

Frequency-based filtering Up to three non-ref alleles were present for Indels. Frequencies for each non-reference allele were extracted and analyzed separately. For SNPs, only one site with more than one non-reference allele was found for both experiments. The second non-reference allele at the SNP site in the 1-Freeze Thaw experiment was present only in one of the control samples. The SNP site with more than one non-reference allele in the 3-Freeze Thaw experiment had low depth of coverage, exceeding 10 in only one sample with only one or two reads for the alternate allele.
To obtain frequencies of the first non-ref allele for each variant, we used the following query:

```
bcftools query -f "%CHROM %POS %REF[ %AD{1}/%DP]\n" <snps_pass.vcf>
```

For others with n alleles:

```
bcftools view -i 'N_ALT>=n' <indels_pass.vcf> | bcftools query -f "%CHROM %POS %REF[
↪  %AD{n}/%DP]\n"
```

A 95% confidence interval for each frequency estimate was obtained to determine whether a significant change occurred in the frequency of a variant in any sample during the course of the evolution experiment. Given the observed frequency of the variant in a sample of reads, the likelihood of different values for the true population frequency was evaluated assuming a binomial distribution of variant read counts. A minimum requirement of 10 total reads at a position was imposed to estimate frequency intervals. The minimum and maximum frequency values at which the probability of observed count falls below 5% constitute the limits of the confidence interval. Only the variants satisfying this condition in the reference as well as in the majority of samples were retained. Where the non-ref allele was already at almost 100% frequency in the parent, the frequency of the reference allele was followed instead. A mutant was removed if its frequency never exceeded 1%. A site was considered invariant if the upper estimate corresponding to its lowest frequency was greater than the lower estimate of its highest frequency. All invariant sites and sites where the minimum frequency change did not exceed 20% in any sample were excluded. The selected variant positions were pooled over experiments, the corresponding variants extracted from the raw VCF, and annotated using snpeff with a locally-built snpeff database for the reference assembly used in this study.

Frequency-based clustering of variants Multiple variants may be present in the same cellular lineage, in which case their frequencies would be expected to change together across samples. Using the confidence intervals on frequencies as estimated above, a distance was calculated between pairs of sites as the sum of the minimum difference between estimated frequencies over samples. Pairs with distance < 0.04 were considered as members of the same cluster. If a variant that occurred across clusters was associated with different variants across clusters, the associated variants were expected to be insignificantly contributing to the selected phenotype. Hence, independent variants or variants that were independently a part of one or more clusters were selected as the final variants.

Frequency-trajectory-based clustering of variants The trajectories of the frequency of each variant were assessed across the parent, mid-point, and final samples. The variants for which the frequency trajectory fluctuated were filtered out. Only those variants whose frequency monotonically increased or decreased across the trajectory were retained.

Intracellular trehalose measurements

Intracellular levels of trehalose were measured based on a previously described protocol (5). During evolution of freeze-thaw tolerance, cell colonies were collected in microcentrifuge tubes from plates used to measure CFU 48 hours after thawing. Cells were weighed and suspended in 0.25 ml of 0.25M sodium carbonate. For measurements after the evolution experiment, 500ul of stationary phase culture was centrifuged at 3000 rcf for 2 minutes to remove media. The cell pellet was then washed with Phosphate Buffered Saline and suspended in 0.25 ml of 0.25M sodium carbonate.
The tubes were gently sonicated for a minute and then incubated at 95°C for 4 hours to lyse the cells and break down all existing glucose. The suspension was buffered to pH 5.2 by adding 0.15 ml of 1M acetic acid and 0.6 ml

Gene	Function	k_{FT} = 1 Rep 1	k_{FT} = 1 Rep 2	k_{FT} = 1 Rep 3	k_{FT} = 1 Rep 4	k_{FT} = 3 Rep 1	k_{FT} = 3 Rep 2	k_{FT} = 3 Rep 3	k_{FT} = 3 Rep 4
Cln3	Cyclin							S	
Pho3	Phosphate metabolism								S
Ho	Homothallic switching endonuclease			NS	NS				NS
SCEN_L05230	Unknown	NS							
Itr1/Itr2	Myo-inositol transporter	NS							
Bch2/Chs6	Chitin Synthase-related				NS				
Vac8	Vacuolar inheritance			FS	FS				
Ade5,7	De novo purine nucleotide pathway			NS					NS
SCEN_J00260	Unknown			IG					
Alr1	Aluminum Resistance				NS				
Dnf1/Dnf2	Aminophospholipid translocase		NS						
Pma1	Plasma Membrane ATPase		NS		NS				
Yeh1/Yeh2	Yeast steryl ester hydrolase				IG				
SCEN_L03720	Unknown								NS
Cbk1	Cell wall biosynthesis kinase						*		
Alg8	Asparagine-linked glycosylation				S				
Ras1/Ras2	Adenylate cyclase activating GTPase	NS	NS			NS	NS	NS	
Rpc82	RNA polymerase C subunit					NS			

Figure S4. List of genetic mutations across all replicates including both the $\mathrm{k_{FT}} = 1$ and $\mathrm{k_{FT}} = 3$ selection regimes. FS - Frame Shift, * - Stop Codon, NS - Non-Synonymous, S - Synonymous, IG - Inter-genic region

of 0.2M sodium acetate for trehalase activity. The mixture was then incubated with 0.025U/ml trehalase (Sigma-Aldrich, Catalog no. - T8778) at 37°C overnight with shaking to break down trehalose into two glucose molecules. The suspension was then centrifuged at 16,900g for 5 minutes and the supernatant was assayed for glucose using a glucose assay kit (Sigma-Aldrich, Catalog no. - GAGO20). The glucose assay was performed using a 96-well plate. 40 μl of the appropriately diluted supernatant was added to each well so that the glucose concentration was within the dynamic range of the assay (20-80 mg/ml). The plate was incubated for 5 minutes at 37° C, followed by the addition of 80ul of the assay reagent to each well to start the colorimetric reaction. The plate was then incubated at 37° C and the reaction was stopped after 30 minutes by adding 80ul of 12N sulfuric acid to each well. The absorbance of each well was measured at 540 nm to calculate the concentration of glucose (and therefore trehalose) from a standard curve.

Modelling Trehalose Dependent Selection

We model the freeze-thaw adaptation by assuming trehalose produced at stationary phase to be the primary phenotypic marker. We assume that the growth rate of cells, the probability of a cell going into quiescence in stationary phase, the probability of survival under a freeze - thaw cycle, as well as the duration of lag time before re-entry into the cell cycle, depend on this stationary phase trehalose concentration.

We start with a population of N individual cells whose intracellular trehalose amount in stationary phase, given by τ, is drawn initially from a Gaussian distribution with mean τ_0 and a narrow peak of with standard deviation σ_τ^0. We take the simplest assumption for the dependence of each cell's growth rate (or fecundity per unit time in the simulation) on stationary phase trehalose concentration,

$$g(\tau) = g_0(1 - \tau/\tau_g) \tag{S5}$$

where g_0 is the highest achievable growth rate and τ_g the amount of trehalose that inhibits growth to effectively zero. At each time step in the growth process, we calculate the number of offspring for each cell according to the above equation, and add them to the population. Each offspring is also subject to a small mutation, which acts to change the trehalose concentration of the offspring with respect to its parent. This mutational effect on offspring trehalose is drawn from a Pearson Distribution at a mutation rate m for each offspring. The distribution has a mutational standard deviation σ_m, a kurtosis k_m and no skew. Thus, most mutations have no effect upon the offspring's trehalose, preserving the value inherited from the parent cell. Simultaneously, some large effect mutations, both positive and negative are possible.

For each division, we assume a constant amount of a finite resource is consumed. This continues till the resource runs out and the population faces resource exhaustion. Upon starvation, yeast forms a heterogeneous population of

quiescent and non-quiescent cells. We model the switch to quiescence as a stochastic process, where the probability of each cell going into quiescence is given by

$$p_q(\tau) = \frac{1}{(1+\exp^{-(\tau-\tau_q)/\gamma_q})}, \tag{S6}$$

where τ_q is the trehalose concentration at which probability of quiescence is 50% and γ_q is a parameter quantifying how quickly the probability rises to 1 as τ increases. For each cell we decide the fate of the cell by comparing this probability with a randomly generated number.If the probability given by S6 is higher than the random number the cell goes into a quiescent state. Upon freezing, the non-quiescent population entirely perishes. Among the quiescent cells, the cells with trehalose concentration above a cut off survive, since trehalose has been shown to be correlated with higher survival to stress even in exponential phase (6). We model the probability of survival,

$$p_s(\tau) = \frac{1}{(1+\exp^{-(\tau-\tau_s)/\gamma_s})}, \tag{S7}$$

where τ_s is the trehalose concentration at which probability of survival under freeze thaw is 50% and γ_s is a parameter quantifying how quickly the probability rises to 1 as τ increases. In general we assume that $\gamma_s < \gamma_q$ and $\tau_s > \tau_g$ since the freezing process is a harsher stress than nutrient scarcity in stationary phase. Thus, both quiescence and the freeze thaw process shift the mean trehalose of the population to higher values since cells with lower trehalose amounts perish.

When the surviving population is allowed to thaw and re-introduced into a growth medium, the cells with higher trehalose concentrations have a shorter lag time, and begin to grow earlier as trehalose is crucial for re-entry into the cell cycle (7). Longer lag times mean less resource available for growth because a small amount of resource is consumed even in the lag phase and the amount depends on the length of the lag phase. We again assume a linear relationship between the lag time and trehalose amounts,

$$l(\tau) = l_0(1-\tau/\tau_l), \tag{S8}$$

where l_0 represents the maximum lag time possible, and τ_l the trehalose value at which the lag time reduces to zero. In each growth cycle, a higher trehalose value thus means a shorter lag phase, and more time available for growth, while simultaneously causing a lower growth rate. Lastly, we model the dilution process of the experimental setup by randomly selecting a fraction d of the population. This can introduce additional stochasticity into the evolution process.

At lower values of trehalose, the effect of a lower growth rate is not sufficient to stop the increase in mean trehalose of the population caused by a shorter lag phase. Cells with higher trehalose are able to produce a larger number of offspring and take over the population.

As the population undergoes another round of growth and glucose exhaustion, we once again have a heterogeneous population, with the distribution of quiescent cells now having a higher mean amount of trehalose production. A larger proportion of the cells are now able to survive the freeze-thaw process because of this upward shift. Hence, our simulation includes both a component of trehalose-dependent stochastic switching to quiescence, as well as growth and lag mediated selection for higher trehalose levels. The trade-off between the decrease in growth rate and the positive effect on all other factors from increasing trehalose sets the final equilibrium value of trehalose in the simulations. The effect of a lower growth rate begins to dominate at larger trehalose values, causing the mean trehalose of the population to stagnate.

Since the increase in the mean trehalose for the population is driven entirely by new beneficial mutations, the trajectory of individual replicates shows many jumps in the mean trehalose. The averaging over several replicates smoothens out the curve since the mutations, and the resulting sweep of the population can occur at different time points. Parameter values used in our simulation can be found in Table 3.

1. Steven B. Haase and Steven I. Reed. Improved flow cytometric analysis of the budding yeast cell cycle. *Cell cycle (Georgetown, Tex.)*, 1(2):117–121, 2002. doi:10.4161/cc.1.2.114.
2. Oliver Otto, Philipp Rosendahl, Alexander Mietke, Stefan Golfier, Christoph Herold, Daniel Klaue, Salvatore Girardo, Stefano Pagliara, Andrew Ekpenyong, Angela Jacobi, Manja Wobus, Nicole Töpfner, Ulrich F. Keyser, Jörg Mansfeld, Elisabeth Fischer-Friedrich, and Jochen Guck. Real-time deformability cytometry: on-the-fly cell mechanical phenotyping. *Nature methods*, 12(3):199–202, 3 2015. URL: http://www.ncbi.nlm.nih.gov/pubmed/25643151, doi:10.1038/nmeth.3281.
3. Alex N. Salazar, Arthur R.Gorter de Vries, Marcel van den Broek, Melanie Wijsman, Pilar de la Torre Cortés, Anja Brickwedde, Nick Brouwers, Jean Marc G. Daran, and Thomas Abeel. Nanopore sequencing enables near-complete de novo assembly of Saccharomyces cerevisiae reference strain CEN.PK113-7D. *FEMS Yeast Research*, 17(7):1–11, 2017. doi:10.1093/femsyr/fox074.
4. Heng Li. Improving SNP discovery by base alignment quality. *Bioinformatics (Oxford, England)*, 27(8):1157–8, 4 2011. URL: https://academic.oup.com/bioinformatics/article/27/8/1157/227268http://www.ncbi.nlm.nih.gov/pubmed/21320865http://www.pubmedcentral.nih.gov/articlerender.fcgi?artid=PMC3072548, doi:10.1093/bioinformatics/btr076.
5. Cihan Erkut, Vamshidhar R Gade, Sunil Laxman, and Teymuras V Kurzchalia. The glyoxylate shunt is essential for desiccation tolerance in C. elegans and budding yeast. *eLife*, 5:1–24, 4 2016. URL: http://elifesciences.org/lookup/doi/10.7554/eLife.13614https://elifesciences.org/articles/13614, doi:10.7554/eLife.13614.
6. Hugo Tapia, Lindsey Young, Douglas Fox, Carolyn R. Bertozzi, and Douglas Koshland. Increasing intracellular trehalose is sufficient to confer desiccation tolerance to Saccharomyces cerevisiae. *Proceedings of the National Academy of Sciences*, 112(19):6122–6127, 5 2015. URL: http://www.ncbi.nlm.nih.gov/pubmed/25918381http://www.pnas.org/lookup/doi/10.1073/pnas.1506415112http://www.pubmedcentral.nih.gov/articlerender.fcgi?artid=PMC4434740https://pnas.org/doi/full/10.1073/pnas.1506415112, doi:10.1073/pnas.1506415112.
7. Lei Shi, Benjamin M. Sutter, Xinyue Ye, and Benjamin P. Tu. Trehalose Is a Key Determinant of the Quiescent Metabolic State That Fuels Cell Cycle Progression upon Return to Growth. *Molecular Biology of the Cell*, 21(12):1982–1990, 6 2010. URL: https://www.molbiolcell.org/doi/10.1091/mbc.e10-01-0056, doi:10.1091/mbc.e10-01-0056.

Table 3. Parameter values for simulations.

N	5×10^4
τ_0	500
σ_τ^0	1
σ_m	2
k_m	200
l_0	6
τ_l	800
g_0	10
τ_g	1200
γ_q	100
τ_q	500
γ_s	50
τ_s	700
d	30